Spectral evolution and probability distributions of surface ocean gravity waves and extreme waves.

Doctor Scientarum Thesis

Hervé Socquet-Juglard

Department of Mathematics
University of Bergen

November 2005

Preface :

This thesis submitted for the degree of Dr. Scient. at the University of Bergen consists of one introduction, two journal articles and one conference paper.

The work presented in this thesis has been performed at the University of Bergen, department of applied mathematics.

I wish to express my gratitude to both professors Kristian Dysthe (University of Bergen) and Karsten Trulsen (University of Oslo) for their guidance and personnal support. Their patience and their enthousiam were greatly appreciated.

Professor Harald Krogstad and PhD Student Jingdong Liu (NTNU) are gratefully acknowledged for their advices in statistic.

I especially thank Bjørn Tore Sund for helping me with computer problems.

This thesis has been supported by a grant from the BeMatA program of the Research Council of Norway, and by support from NOTUR and Norsk Hydro.

Statoil is acknowledged for financial support during the last six months.

Finally, I will thank my family and all my friends from France and Norway for their support during this work.

Contents

1 Introduction

One of the first things a man will notice when looking at the ocean is the presence of waves. More than 2.000 years ago, Aristotle knew already that the interaction between the air and and sea surface was playing an important role in the formation of ocean waves. However, very little progress had been made from the ancient Greeks to the 19th century. Airy (1801-1892), Stokes (1819-1903) and Rayleigh(1842-1919) are among the scientists who gave important contributions to the knowledge of ocean waves. Generally, ocean surface waves are the result of forces acting on the ocean. Starting from a physical point of view, we will build a classification of ocean waves by their wave period and their physical mechanism. In nature, several types of ocean waves can be observed. In space, a wave can be high, short, long, small, symmetric, asymmetric, periodic ... In time, a wave can be fast, slow, ... The presence of waves in the oceans can be explained by different physical mechanisms :

- Water compressibility which leads to the creation of sound waves that are of no interest in this present thesis.
- Pressure or stress from the atmosphere (particularly through the wind) create capillary and gravity waves.
- Submarine earthquake creating very long surface gravity waves. The last example the whole world has in mind is the tsunami that took place in Asia the 26th of December. More than 100.000 people died. The earthquake created a long wave of small amplitude travelling very fast in the deep ocean. While the wave approached shallow areas on the continental shelves, it slowed down and increased in amplitude. This wave even killed some hundred people at the east African coast, thousands of kilometers away from the earthquake.
- Gravitational attraction from the moon and rotation (Coriolis force) of the earth generate tidal waves.

Wave type	Wave Period	Physical mechanism
Capillary wave	0-0.1s	Surface shear
Gravity capillary wave	0.1-1s	Surface shear, wind
Gravity wave	1-min	Wind, gravity
Seiche	5-40 min	Wind variation
Tsunami	30 min - 12 h	earthquake
Tidal waves	12-24 h	Action of the moon and the sun and the Coriolis force

Non natural physical event can also produce waves in the ocean. One can take the example of a boat cruising in a fjord. Depending of its speed and the depth of the fjord, the boat can generate waves which become high enough to cause some damages along the coast.

Ocean surface waves have been a subject of study with increasing interest the last 50 years. Shipping companies, offshore industries (especially the oil and gas producers), fish industries (fish farms, ...), harbours (transport of sediments), tourist industry (ships, waves breaking on beaches, ...) and environmentalists are more and more concerned about the role of the waves on the ocean. A better understanding of the waves can play a major role in the economy, the safety of populations and the protection of the world. A wave hitting an oil platform and stopping the production of oil means several millions of U.S. dollars lost per day for the company. When a tsunami reaches a coast without warning, thousands of human lives may be lost. We can increase the list of examples where waves play a major role in the daily world. In the present thesis, we shall focus on the so-called freak wave, also named rogue wave or extreme wave. These waves are storm waves with extreme heights compared to the average. In this short introduction, we focus on waves in general and a more precise definition of a freak wave will be given later.

Before entering more into details on waves, we need to make some basic assumptions about the ocean :

- The water is incompressible.
- The water has an inviscid nature meaning friction is neglected. Only gravity and pressure forces are taken into account.
- The fluid is irrotational.

Observing the ocean from a beach, during calm weather, we can notice the presence of nearly sinusoidal, long-crested and progressive waves (see Figure 1). These waves will become higher and shorter when reaching the coast and will finally break. This phenomenon is well-known for the surfers. The wave repeats itself, has a nearly sinusoidal shape and is moving at a constant speed with a direction perpendicular to the crests. The wave is a long series of crests with same heights at the same distance from each other.

Let us give some definitions in wave theory referring to Fig.(2):

- The surface elevation $\eta(\boldsymbol{x}, t)$ is the vertical deviation from the equilibrium surface $\eta = 0$.
- An upcrossing wave is a wave between two successive mean level upcrossings (X2 and X4 on the figure).

Figure 1: View from a beach of sinusoidal waves. Copyright www.tim-mckenna.com

- A downcrossing wave is a wave between two successive mean level downcrossings (X1 and X3).
- The wave crest Ac is the maximum value (C2) between a mean level upcrossing (X2) and the next downcrossing (X3).
- The wave trough At is the minimum value (T1) between a mean level downcrossing (X1) and the next upcrossing (X2).
- The wave height H is the crest-to-trough vertical distance.

For periodic waves :

- The wavelength λ is the length between two successive wave crests.
- The period T is the time between two successive wave crests pass a fixed point.
- The phase speed c is the speed of the wave crests.
- The wavenumber k is the number of crests per unit distance and is equal to $2\pi/\lambda$.
- The angular frequency ω is the number of radians per second and is equal to $2\pi/T$.
- The wave profile of a sinusoidal wave is therefore

$$\eta(x,t) = a\sin(kx - \omega t) \tag{1}$$

where a is the amplitude and $\theta = kx - \omega t$ is called the phase.

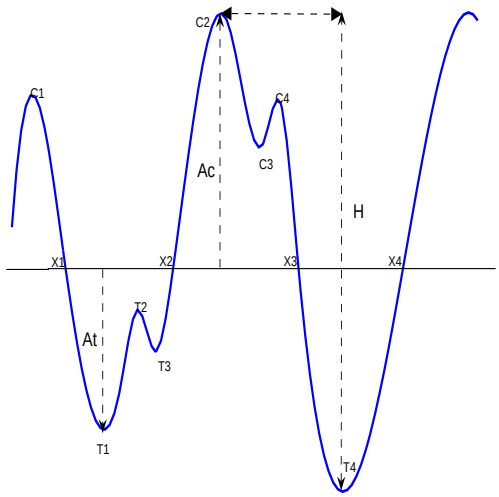

Figure 2: Description of some wave parameters.

The water depth h plays a major role in ocean physics. When a wave propagates, both surface and underwater particles are in motion. The phase speed and the frequency of the waves depends on depths. Simple classifications using the water depth and the wavelength to characterize the ocean have been made (see for example [1])

- Shallow water $h < \lambda/25$;
- Transitional depth $\lambda/25 < h < \lambda/4$;
- Deep water $\lambda/4 < h$.

In the present thesis, we will work under the assumption of deep water. It's now time to introduce a fundamental relationship between the wavenumber k and the wave frequency ω which is called the dispersion relation. From linearized theory, this relation can be easily derived :

$$\omega^2 = gk \tan(kh) \tag{2}$$

where g is the gravitational acceleration equal to $9.81 m.s^{-2}$. For deep water, $\tan(kh) \approx 1$ and the dispersion relation reduces to $\omega^2 = gk$.

It's obvious when watching the ocean that the sea is not a single sinusoidal wave. Looking at the sea, it's not easy to get a general description or law of the surface elevation. The sea surface looks pretty confused. Waves have different speeds, amplitudes, directions, wavelengths, ... Short waves ride on top of the long waves and small waves are overtaken by longer waves. It seems that the sea surface evolves almost randomly if

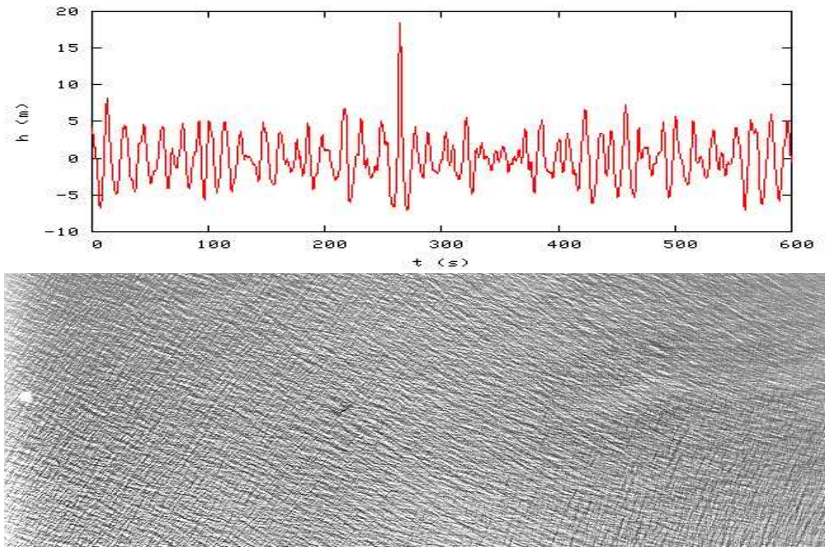

Figure 3: a) Surface elevation at one point of the ocean. Here it's the so-called "New Year wave" which hit the Draupner offshore platform the 1st of January 1995. b) Sea surface from a satellite - SAR image.

you look at one particular point of the ocean (see Figure 3a). Looking at a larger piece of the ocean from a satellite, one can see the influence of the wind and the pattern of the waves looks more regular due to the filtering that a finite resolution produces even though the randomness is still there. (see Figure 3b).

However, the ocean can be simulated as the sum of simple sinusoidal waves with different lengths, heights and directions. We start explaining this construction of the ocean with two simple waves. We make the assumption that the two waves have the same height but differ slightly in wavelength. Adding these two waves, we get a wave with non uniform waveheigths and distances between the wave crests. Figure 4 shows the construction of such a wave. In our example, we choose the sine wave (Fig 4a) and a slightly modified sine wave, $\sin(1.1x)$ (Fig 4b). On Fig 4c they are plotted together. Comparing the resulting wave (Fig 4d) with Fig 4c shows that the resulting wave has a local maximum when the two sinusoidal waves are in phase while it's a minimum when they are out of phase. It's interesting to notice that in adding two simple sinusoidal waves, we already get a more complicated wave.

Keeping the same idea, we can superpose a large number of simple sinusoidal waves to build the sea surface. Figure 4 shows the case of two 1D waves added together. Therefore it should not surprise us anymore than adding 2D waves with different heights, wavelengths and directions will result in an ocean where no general laws

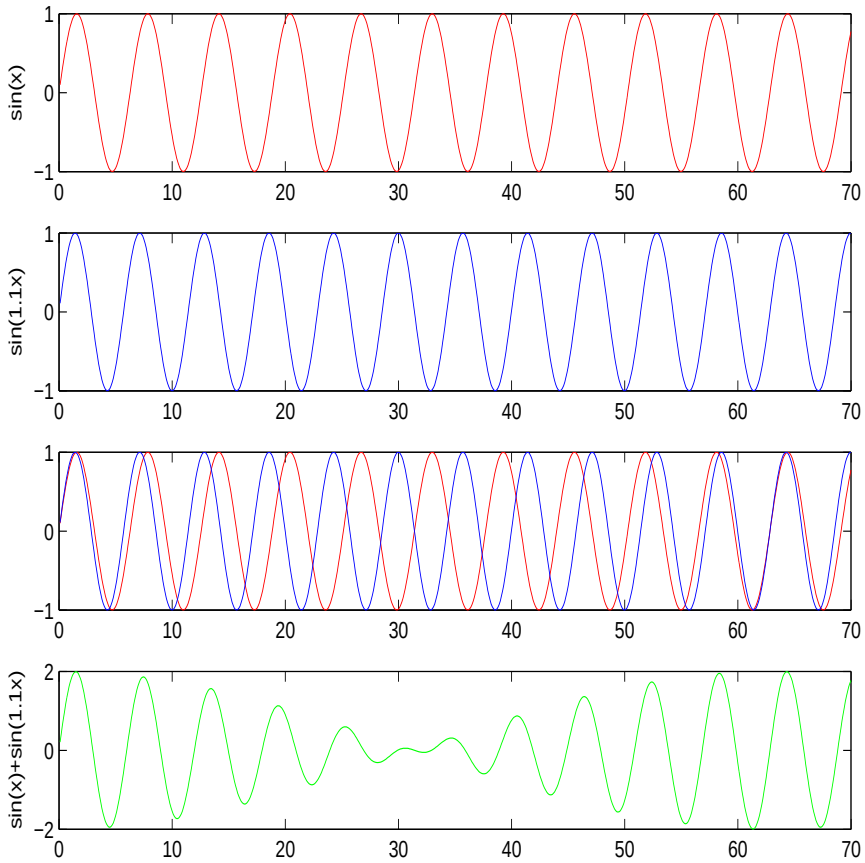

Figure 4: a) $\sin(x)$ b) $\sin(1.1x)$ c) $\sin(x)$ and $\sin(1.1x)$ d) $\sin(x) + \sin(1.1x)$

seem to be observed. Lord Rayleigh said : "The basic law of the seaway is the apparent lack of any law".

From a general result established by Fourier it follows that the sea surface at a given instant can be obtained from the superposition of many simple sinusoidal waves. It's quite fascinating to realise that something very complicated can be gotten by adding very simple elements.

In linear theory, one can simulate the sea surface at any time by adding many sinus waves like

$$\eta = \sum a_n \sin(\boldsymbol{k_n} \cdot \boldsymbol{x} - \omega_n t + \phi_n) \tag{3}$$

with random phases ϕ_n where in deep water $\omega_n = \sqrt{g|\boldsymbol{k_n}|}$. Each sine-wave in the sum is an elementary wave sometimes called a Fourier mode.

Taking non linear effects into account, however, means that the individual Fourier modes are coupled. Thus the amplitudes a_n and phases ϕ_n are changing with time and have to be computed at any time step.

2 Freak waves

We will present in this section some accounts and stories about freak waves which have been related in scientific papers, popular science magazines and even news from press agencies. Waves with hight exceeding 30 meters are reported.
Freak waves in shallow and deep water have been observed all around the world, along the South African Coast, in the Gulf of Mexico, in the North Sea or Japan Sea. Kharif et al. [2] give a small survey of the different explanations of the generations of such abnormal waves. In linear theory, one can cite Lavrenov [3] (amplification due to opposing current), White and Fornberg [4] (wave focusing due in a random current) and Pelinovksy and Kharif [5] (wave focusing in arbitrary depth). In nonlinear theory, one can mention Dysthe and Trulsen (see for example [6]) using the Modified Non Linear Schrödinger Equations or Onorato et al. [7] using the Zakharov Equations.

1. **US Navy steamship Ramapo**

   Reported by Lawton [8]
   In February 1933, the US Navy steamship Ramapo ploughed into a Pacific storm en route to Manila from San Diego. The wind howled at an unremitting 60 knots-force 11-for seven days, lifting the sea into huge 15-metre swells. On the morning of 7 February, the ship encountered a monster. It came from behind, tossing her into a deep trough then lifting her stern-first over a mountain of foamy brine. As the stern of the 146-metre ship hit the bottom of the trough, the officer on watch triangulated the wave against the crow's nest. The figure he came up with was 34 meters-about as tall as an 11-storey building. It remains the biggest wave ever reliably measured.

2. **Cruiser Line Queen Elizabeth II**

   Reported by E.S.A. (European Space Agency) [9]
   In February 1995 the Cruiser Line Queen Elizabeth II met a 30-meter high rogue wave during a hurricane in the North Atlantic that Captain Ronald Warwick described as "a great wall of water... it looked as if we were going into the White Cliffs of Dover."

3. **The Bremen and the Caledonian Star**

   Reported by E.S.A. (European Space Agency) [9]
   The week between February and March 2001 two hardened tourist cruisers - The Bremen and the Caledonian Star - had their bridge and windows smashed by 30-meter waves in the South Atlantic, the former ship was left drifting without navigation or propulsion for a period of two hours.

Wolfgang Rosenthal (senior scientist - Germany) : "All the electronics were switched off on the Bremen as they drifted parallel to the waves, and until they were turned on again the crew were thinking it could have been their last day alive. The same phenomenon could have sunk many less lucky vessels: two large ships sink every week on average, but the cause is never studied to the same detail as an air crash. It simply gets put down to 'bad weather'."

4. **Statoil rig**

   The 1st of January 1995, the Draupner oil rig owned by Statoil in the North Sea has registered a 25.6 meters wave (see Figure 3a). The same year, in the North Sea, Statoil floating rig Veslefrikk B is severely damaged by a rogue wave. One crew member describes a "wall of water" visible for several minutes before it strikes.

5. **Yachtswoman Isabelle Autissier**

   In 1994, the yachtswoman Isabelle Autissier capsized off the coast of New Zealand when she hit one of these monsters which she estimated to be 35 metres high.Isabelle Autissier recounts her Southern Ocean scare : "It went right over through 360 degrees. I fell on the bulkhead, then on the ceiling, and back on the other bulkhead. When I opened my eyes the boat was full of water."

   Dan Dickison [10] has reported : "Huddled in the cold, dark confines of her wrecked Ecureuil Poitou-Charentes 2, the 39-year-old mariner was helplessly adrift after an enormous wave on the storm-frothed Indian Ocean sent the 60-foot yacht into a 360-degree roll. Autissier, who had avoided injury by wedging herself into a small passageway, emerged to find her masts broken and the cabin top shorn away, leaving a Renault-size hole in the deck that flooded part of the boat with icy seawater."

   John Vigor [11] wrote : "When Isabelle Autissier's 60-foot racer capsized in the Southern Ocean, it sent a chill of fear through the sailing community. Sailors don't like to think of capsize. But here was a big, well-found boat, a Finot-designed Open 60 Class flier, wallowing upside down in huge frigid swells, with her long thin keel jutting toward heaven. It was a bizarre and frightening sight.

   Autissier was lucky. She was taking part in the Around Alone race, so her million-dollar boat was equipped with emergency satellite transmitters, position recorders, and lots of other equipment that no normal cruiser is likely to be

able to afford or fit on board. She was eventually rescued in a wonderful feat of seamanship by Giovanni Soldini, a fellow competitor."

6. **Oil tankers damaged by giant waves off the south-east coast of South Africa**

   Ronald Smith [12] has collected several ship accident due to freak waves :
   "During the closure of the Suez Canal a number of ships, particularly oil tankers, have reported extensive damage caused by giant waves off the south-east coast of South Africa (Mallory 1974; Sturm 1974; Sanderson 1974). Two particularly unfortunate vessels are the World Glory, which broke in two and sank in June 1968, and the Neptune Sapphire, which lost 60 m of its bow section in August 1973. we can only speculate that giant waves may account for many of the ships which have been lost without trace off this coast."

7. **Oil tanker Esso Languedoc**

   The story is reported by Graham Lawton [8].
   "We were in a storm and the tanker was running before the sea. This amazing wave came from the aft and broke over the deck. I didn't see it until it was alongside the vessel but it was special, much bigger than the others. It took us by surprise. I never saw one again." Philippe Lijour, first mate of the oil tanker Esso Languedoc, describing the huge wave that slammed into the ship off the east coast of South Africa in 1980.

   Lijour and his shipmates are lucky to be alive. They were struck by a rogue wave-a monstrous wall of water that rose out of nowhere and slammed onto the deck like the fist of god. Ships often don't survive an onslaught like that. Many sink before anyone on board knows what's hit them. Lijour had another stroke of luck that day. As the wave crashed into the ship, he managed to grab his camera. The photograph he took, is one of the few images we have of a rogue wave (see Fig.5). It shows a monstrous wall of foam-flecked water, much bigger that anything else on the sea at the time, smashing into the ship's starboard bow. By comparing it to the ship's masts, Lijour estimates that the wave was around 20 meters high. In truth it was probably bigger. Rogue waves are often preceded by a deep trough, so viewed from the sea surface shortly before it struck, the wave could have towered 30 meters or more. It would have been like being hit by a department store.

8. **M/S "Norse Variant" and M/S "Anita"**

   These two events have been reported by Kjeldsen [13].
   "Loss of a large Norwegian ship with entire crew in the middle of the North

Figure 5: Picture of a Rogue wave taken by Philippe Lijour on board of the oil tanker Esso Languedoc in 1980.

Atlantic is not a common event. However at a special occasion two large Norwegian bulk ships M/S "NORSE VARIANT" and M/S "ANITA" disappeared at the same time and in the same area. Both ships passed Cape Henry with only one-hour interval in time on voyages from the U.S.A to Europe. Both ships came right into the centre of a very extreme weather event with a strong low pressure giving 15 m significant wave heights and mean wave periods close to 10 seconds and strong northerly winds with wind velocities near 60 knots. "NORSE VARIANT" had deck cargo that was damaged and moved by water on deck with the result that a hatch cover was broken and left-open. The ship took in large amounts of water and sank before an organised evacuation was finished. Only one member of the crew was rescued on a float.
"ANITA" disappeared completely at sea with the whole crew and no emergency call was ever given. The Court of Inquiry then concluded that the loss can be explained by an event in which a very large wave suddenly broke several hatch cover on deck, and the ship was filled with water and sank before any emergency call was given.
The wave that caused the loss of "ANITA" was probably a freak or rogue wave.

9. **Tanker World Glory and some references.**

   Lavrenov in [3] reports that : "On 13 June 1968 the tanker World Glory (built in the U.S.A. in 1954) under the Liberian flag while travelling along the South African coast, encountered a freak wave, which broke the tanker into two parts and led to the death of 22 of its crew members."
   He also gives a list of interesting authors describing the same kind of events, especially Mallory [14] who describes 11 cases of vessels who had encountered abnormal waves along the South African coast. However, it seems that some of the cases given by Mallory are not really due to freak waves.

10. **SS Spray**

    Captain G. Anderson Chase was on board the SS Spray (ex-Gulf Spray) in February of 1986, in the Gulf Stream, off of Charleston when the picture (see Fig. 6) was taken.
    He wrote [15]: "A substantial gale was moving across Long Island, sending a very long swell down our way, meeting the Gulf Stream. We saw several rogue waves during the late morning on the horizon, but thought they were whales jumping. It was actually a nice day with light breezes and no significant sea. Only the very long swell, of about 15 feet high and probably 600 to 1000 feet long. This one hit us at the change of the watch at about noon. The photographer was an engineer (name forgotten), and this was the last photo on his roll of film.

Figure 6: Picture of a big wave taken on board of the SS Spray in 1986.

We were on the wing of the bridge, with a height of eye of 56 feet, and this wave broke over our heads. This shot was taken as we were diving down off the face of the second of a set of three waves, so the ship just kept falling into the trough, which just kept opening up under us. It bent the foremast (shown) back about 20 degrees, tore the foreword firefighting station (also shown) off the deck (rails, monitor, platform and all) and threw it against the face of the house. It also bent all the catwalks back severely. Later that night, about 19.30, another wave hit the after house, hitting the stack and sending solid water down into the engine room through the forced draft blower intakes."

11. **Taganrogsky Zaliv**

In 1985, the Russian ship Taganrogsky Zaliv (164.5 meters long) was cruising along the South African Coast. The ship encountered a freak waves and a seaman was killed. Lavrenov in [3] gives us the weather details and what happened on the foredeck.

"Near the Cape of Good Hope, the possibility of encountering a weather storm is high enough, so the ship was prepared for sailing in stormy weather. The north-north east wind was blowing at a speed of 7 m/s. At 5 a.m., it changed direction to south-south west with the same force. From the previous day the atmospheric pressure was diminishing until the wind change direction, after that it began to increase. At 8.00 a.m., the wind became stronger and at 11 a.m it reached 15 m/s. By the noon of the day everybody felt the wave impact of the ship, which tore off a lifeboat, loosend two mooring-line reels and washed them into water.

After 12.00, the wind speed diminished to 12 m/s. Wind sea became calmer as well. The wind force didn't change during the next three hours. Wave height didn't exceed 5 m and the length was 40-45 m. To overcome the results of the wave impact, the boatswain and three seamen were sent out to the foredeck. The speed of the ship was diminished to a minimum that was enough for safe control of the ship's motion. The ship rode well on the waves. The foredeck and main deck were not flooded with water.

By one o'clock, the job was almost done on the foredeck. At the moment, the front part of the ship suddenly dipped, and the crest of a very large wave appeared close to the foredeck. It was 5-6 m higher than the foredeck. The wave crest fell down on the ship. One of the seamen was killed and washed overboard. It was impossible to save him.

Nobody was able to foresee the appearance of the wave as the weather was normal for ocean conditions. When the ship went down, riding on the wave, and burrowed into its frontal part, nobody felt the impact of the wave. The wave

easily rolled over the foredeck, covering it with more than two meters of water. The length of the wave crest was no more than 20 m."

12. **Norwegian Dawn**

NEW YORK (AP) [16] – A cruise ship struck by a freak seven-story-high wave that smashed windows and sent furniture flying returned to New York Harbor on Monday and docked at its berth on the Hudson River.
The 965-foot white ocean liner was sailing back to New York from the Bahamas when it was struck by a storm Saturday, the 16th of April 2005, that pounded the vessel with heavy seas and the rogue 70-foot wave.
The wave sent furniture sailing through the air and knocked Jacuzzis overboard. Some passengers slept in hallways in life jackets.
"The ship was hit by a freak wave that caused two windows to break in two different cabins," Norwegian Cruise Line said in a statement. It said 62 cabins were flooded and four passengers had cuts and bruises. The wave reached as high as deck 10 on the ship, company spokeswoman Susan Robison said Sunday.
The Norwegian Dawn docked at Charleston for repairs and a Coast Guard inspection before continuing its voyage to New York early Sunday.
Bill and Ellen Tesauro of Wayne, New Jersey, said they went to the ship's casino when the storm started slamming the vessel.
"We figured it would take our minds off this (and) that's when the captain announced that drinks are free all night," Bill Tesauro told the Daily News of New York. "But then there was another horrendous slap on the water."
The panicked couple returned to their suite.
"A desk went flying across the room," Ellen Tesauro said. "And a glass table toppled down, with glasses and food on it."
Stacy Maryland of Hamilton, New Jersey, woke up to find shoes and magazines floating in a foot of water.
"I thought I heard water sloshing around, and then I woke up and saw it, and it was surreal," she told the newspaper.
The cruise line said passengers whose cabins were flooded were flown home from Charleston and the safety of the ship "was in no way compromised by this incident."

3 Equations

Freak waves have been associated with some well-known equations as the Schrödinger equation or the Zakharov equations. Our work uses mainly the modified form of the Schrödinger Equation developed by Dysthe [17]. In this part, we will show how these equations are obtained.

A fluid can be described by its velocity $\boldsymbol{v}(x, y, z, t)$ and its surface displacement $\eta(x, y, z, t)$. We have introduced the Cartesian coordinates (x, y, z) where $\boldsymbol{x} = (x, y)$ and z are respectively the horizontal and vertical coordinates. We use two different operators. ∇ is the gradient defined by $\boldsymbol{i}\frac{\partial}{\partial x} + \boldsymbol{j}\frac{\partial}{\partial y} + \boldsymbol{k}\frac{\partial}{\partial z}$ and $\triangle$ is the Laplacian defined by ∇^2. ($\boldsymbol{i}, \boldsymbol{j}$ and $\boldsymbol{k}$) are unit vectors.

We first assume that our fluid is incompressible and of homogeneous density ρ. Using the mass conservation

$$\frac{d\rho}{dt} + \rho\nabla \cdot \boldsymbol{v} = 0, \tag{4}$$

we deduce that ($\nabla \cdot \boldsymbol{v} = 0$). The flow is assumed to be irrotational ($\nabla \times \boldsymbol{v} = 0$) Therefore we can write that the Laplacian of the velocity potential ϕ is equal to zero everywhere where $\boldsymbol{v} = \nabla\phi$. No flux is imposed at the bottom. On the free surface both kinematic and dynamic conditions must be satisfied. The kinematic condition states that the mass flux through the surface is zero. The dynamic condition expresses the continuity of pressure across the free surface. Therefore we obtain the following system of equations in the Cartesian coordinates (x, y, z):

$$\triangle\phi = 0 \qquad \text{for } -h < z < \eta(x, y, t), \tag{5}$$

$$\phi_t + \frac{1}{2}(\nabla\phi)^2 + g\eta = p(t) \qquad \text{at } z = \eta(x, y, t), \tag{6}$$

$$\eta_t + \phi_x\eta_x + \phi_y\eta_y - \phi_z = 0 \qquad \text{at } z = \eta(x, y, t), \tag{7}$$

$$\phi_z = 0 \qquad \text{at } z = -h \tag{8}$$

g is the acceleration of gravity and $p(t)$ is the atmospheric pressure. We assume a definition of ϕ such as $p(t)$ will be included in ϕ_t.

Taking the total derivative of 7 and using the dynamic condition, we then get the new system of equations for describing the surface waves :

$$\triangle\phi = 0 \qquad \text{for } -\infty < z < \eta(x,y,t), \tag{9}$$

$$\phi_{tt} + g\phi_z + (\nabla\phi)_t^2 + \frac{1}{2}\nabla\phi\cdot\nabla(\nabla\phi)^2 = 0 \qquad \text{at } z = \eta(x,y,t), \tag{10}$$

$$\eta_t + \phi_x\eta_x + \phi_y\eta_y - \phi_z = 0 \qquad \text{at } z = \eta(x,y,t), \tag{11}$$

$$\phi_z = 0 \qquad \text{at } z = -h \tag{12}$$

We introduce the harmonic series expansions for the potential ϕ and the surface elevation η for a slow evolution of the wavetrain :

$$\phi = \bar{\phi} + \frac{1}{2}\sum_{j=1}^{j=\infty}\left(A_j e^{j(k_0 z + i\theta)} + c.c.\right), \tag{13}$$

$$\eta = \bar{\eta} + \frac{1}{2}\sum_{j=1}^{j=\infty}\left(B_j e^{ji\theta} + c.c.\right) \tag{14}$$

where $c.c.$ means the complex conjugate. $\bar{\phi}$ and $\bar{\eta}$ are real function, representing the mean flow and surface elevation brought about by the radiation stress. θ is the phase equal to $\boldsymbol{k_0}\cdot\boldsymbol{x} - \omega_0 t$ where $(\boldsymbol{k_0}, \omega_0)$ is the location where the spectrum is centred. $k_0 = |\boldsymbol{k_0}|$

We work under the following assumptions :

- $k_0 a = O(\varepsilon)$.
- The bandwith restriction $|\triangle k|/k_0 = O(\varepsilon)$.
- We work on deep water meaning that the depth is large in comparison to the wavelength $(k_0 h)^{-1} = O(\varepsilon)$.

where ε is the wave steepness defined by $\varepsilon = k_0 a$, $k_0 = |\boldsymbol{k_0}|$ and a is a characteristic amplitude. Due to bandwith restrictions, the coefficients A_j and B_j are complex and have rates of change $O(\varepsilon)$ in space and time. It implies that the first harmonic of the velocity potential A_1 and the surface elevation B_1, here after denoted A and B, are of order ε, the second harmonics, A_2 and B_2, are of order ε^2,... In a general rule, A_n and B_n are of order ε^n.

By developing 10 and 11 in Taylor series around $z = 0$, we get to the fourth order in ε :

$$L\phi + \eta L\phi_z + \frac{1}{2}\eta^2 L\phi_{zz} + \frac{1}{6}\eta^3 L\phi_{zzz} + (\nabla\phi)_t^2 + \eta\,(\nabla\phi)_{tz}^2 + \frac{1}{2}\eta^2\,(\nabla\phi)_{tzz}^2 + \\ + \frac{1}{2}\nabla\phi\cdot\nabla(\nabla\phi)^2 + \eta\left(\nabla\phi\cdot\nabla(\nabla\phi)^2\right)^2 = 0, \quad (15)$$

$$\eta_t + \phi_z + \nabla_z\cdot(\eta\nabla_z\phi) + \nabla_z\cdot\left(\frac{1}{2}\eta^2\nabla_z\phi_z\right) + \nabla_z\cdot\left(\frac{1}{6}\eta^3\nabla_z\phi_z z\right) = 0 \quad (16)$$

where L and ∇_z are the linear operator $L(f) = f_{tt} + gf_z$ and the horizontal gradient operator $\nabla_z f = (f_x, f_y)$ respectively.

We substitute 13 and 14 into 9, 12, 15 and 16 up to fourth order in ε. Note that $\bar{\phi}$ is a second order quantity and $\bar{\eta}$ is a third order quantity. We also use the following transformations to make the results dimensionless. Note that the parameter ε will not appear explicitely in our new set of equations.

- $\omega t \longrightarrow t$,
- $k(\boldsymbol{x}, z) \longrightarrow (\boldsymbol{x}, z)$,
- $k(B, B_n, \bar{\eta}) \longrightarrow (B, B_n, \bar{\eta})$,
- $k^2\omega^{-1}(A, A_n, \bar{\phi}) \longrightarrow (A, A_n, \bar{\phi})$.

To the fourth order in ε, we get the following evolution equations :

$$B_t + \frac{1}{2}B_x + \frac{i}{8}B_{xx} - \frac{i}{4}B_{yy} + \frac{i}{2}|B|^2 B = \frac{1}{16}B_{xxx} \\ -\frac{3}{8}B_{xyy} - \frac{5}{4}|B|^2 B_x - \frac{1}{4}B|B|_x^2 - iB\bar{\phi}_x \qquad \text{at } z = 0 \quad (17)$$

$$\nabla^2\bar{\phi} = 0 \qquad \text{for } -h < z < 0 \quad (18)$$

$$\bar{\phi}_z = \frac{1}{2}|B|_x^2 \qquad \text{at } z = 0 \quad (19)$$

$$\bar{\phi}_z = 0 \qquad \text{at } z = -h \quad (20)$$

Equations 17-19 is called the Modified Nonlinear Schrödinger (MNLS) Equation. It was first developed by Dysthe [17] and therefore the equation is also called the Dysthe Equation. Dysthe took the perturbation analysis originally used for the derivation of the cubic Schrödinger equation one step further, i.e. to fourth order in the wave

steepness, to derive the MNLS equation. Note that in the original paper of Dysthe, the MNLS equation was expressed in terms of A. If we drop out all the nonlinear terms on the right side of the Equation (17), we get the conventional form of the cubic Nonlinear Schrödinger (NLS) Equation. Another type of deterministic wave propagation model is the Zakharov Integral Equation developed by Zakharov [18]. It's a perturbation expansion of the Euler Equations for small steepness but without any restriction of the bandwith. The MNLS Equation is a particular case of the third order Zakharov Integral Equation. This result has been showed by Stiassnie [19] who emphasizes that it is not a surprise since all the fourth order terms emerge as a result of the narrow spectral width, and none of them is fourth order in the wave amplitude itself. Trulsen [20] gives a non exhaustive survey of deterministic waves propagation models. Models have the following properties : time and space evolution, weakly or exact nonlinear and slowly (narrow-banded) or fast (arbitrary bandwith) modulated.

In this present thesis, we haven't used two other types of equations, which are extensions from the MNLS equation.

- The broader band (BMNLS) equation was obtained by Trulsen & Dysthe [21] by expanding the linear part of the equation to higher order in the spectral width. The bandwith of the BMNLS is assumed to be of order $\varepsilon^{1/2}$.

- The exact linear (ELMNLS) was obtained by Trulsen et al. [22]. It extends the MNLS equation with exact linear dispersion.

Working first on the evolution of a Gaussian spectrum, we didn't notice any differences between the MNLS equation and these two extended MNLS equations. However, it has not been checked for a JONSWAP spectrum and for the statistics of the surface elevation.

4 The numerical scheme

Our main interest is to find the value of the complex amplitude B in the MNLS equation. The numerical scheme implemented by Trulsen and Dysthe (see [23] for example) to solve this problem has been developed by Lo and Mei [24]. There are two main ideas behind this numerical scheme. The first one is to take advantage of the Fast Fourier Transform (FFT) to calculate the value of $\bar{\phi}_x$ at $z = 0$ at any time step. Then, a split-step technique introduced by Tappert [25] in conjunction with the FFT is used to obtain the value of $B(x, y, z, t)$. In this method, the integration of the linear and nonlinear parts of the governing Equation are done successively. The linear part is integrated exactly while the nonlinear part is integrated with a second order explicit scheme.

4.1 The Fast Fourier Transform

The fast Fourier transform (FFT) is a discrete Fourier transform algorithm which reduces the number of computations needed for N points from N^2 to $Nlg(N)$, where lg is the base-2 logarithm.
The discrete Fourier transform of length N (where N is even) can be rewritten as the sum of two discrete Fourier transforms, each of length $\frac{N}{2}$. One is formed from the even-numbered points; the other from the odd-numbered points. Denote the n^{th} point of the discrete Fourier transform by F_n. Then

$$F_n = \sum_{k=0}^{N-1} f_k e^{-2\pi ink/N} \tag{21}$$

$$F_n = \sum_{k=0}^{N/2-1} f_{2k} e^{-2\pi ink/(N/2)} + W^n \sum_{k=0}^{N/2-1} f_{2k+1} e^{-2\pi ink/(N/2)} \tag{22}$$

$$F_n = F_n^{even} + W^n F_n^{odd} \qquad \text{where } W = e^{-2\pi i/N} \text{ and } n = 0,...,\text{N} \tag{23}$$

This procedure can be applied recursively to break up the $N/2$ even and odd points to their $N/4$ even and odd points. If N is a power of 2, this procedure breaks up the original transform into $lg(N)$ transforms of length 1.

4.2 More details about the numerical scheme

Looking at the Equation 17, we can observe that at any time step, the value of the slow drift is required. Using the known value of $B(x, y, t)$ from previous computations, we can solve $\bar{\phi}$ step by step in time by the pseudo spectral method developed by

Fornberg and Whitham [26]. The first step is to express $\bar{\phi}$ and $|B|_x^2$ with their inverse Fourier Transforms. The slow drift is solved by substituting the Fourier Transform of $\bar{\phi}$ and $|B|_x^2$ into the Equations 18,19 and 20 and by taking advantage of the property of the derivative of the Fourier Transform. We get an expression of $\hat{\phi}_{mn}$ as a function of $|\hat{B}(x,t)|_{mn}^2$ (see for example [23] or [24]). It's then easy to get an expression of $\bar{\phi}_x$ at $z = 0$. Then, we are ready to solve 17.

The basic idea was given in [25]. Every time evolution equation can be written as the sum of its linear and nonlinear terms :

$$B_t = L(B) + N(B) \tag{24}$$

where $L(.)$ and $N(.)$ are respectively the linear and the nonlinear operators. This equation can be split into two equations :

$$B_t = L(B) \tag{25}$$

$$B_t = N(B) \tag{26}$$

At each time step both equations are solved successively, employing the solution of the previous one as the initial condition for the next one. Lets having a solution $B(t)$ of 24 at t. We now want to have the solution at $t + \delta t$. The first step is to solve 26 by an implicit finite difference approximation :

$$\tilde{B}(t + \delta t) = B(t) - 0.5\delta t \left[N(\tilde{B}(t + \delta t)) + N(B(t)) \right] \tag{27}$$

The second step is to advance the solution exactly using only the linear terms by taking advantage of the Fourier Transform. Let's note $F(L(B)) = PF(B)$. We get :

$$B(t + \delta t) = F^{-1}(e^{iP\delta t} F(\tilde{B})) \tag{28}$$

where F^{-1} is the inverse Fourier Transform. Trulsen in [20] makes an interesting comment about the order of solving the Equations 25 and 26. If they are solved alternatively (LNLN), one achieves a first order integration scheme provided each linear and nonlinear integration is at least first order. But if we reverse the order as followed (NLLN), one achieves a second order integration scheme provided each linear and nonlinear integration is at least second order.

5 The simulations

We have only been used the MNLS equation of Dysthe, the simplest of the 4th order Schrödinger equations. As stated in [paper 1], there is no significant difference between the results using MNLS and the other types of 4th order Schrödinger Equations developed by [21], [22] & [23]. Simulations have always been performed in deep water. The time range of validity of the MNLS equation, due to our model based on a perturbation equation, is $(\varepsilon^3\omega_0)^{-1}$ (see [21]). A confirmation of this result has been given by Trulsen and Stansberg [27] who made comparisons between the MNLS model and some wave tank experiments of long-crested waves.

5.1 The reconstruction formula

With our model, the surface displacement can be reconstructed up to third order for the MNLS equation (see Figure 7). The reconstruction formulas of 17, 18, 19 and 20 given by Trulsen [20] are :

$$\bar{\eta} = -\bar{\phi}_t \tag{29}$$

$$B_2 = \frac{1}{2}\left(B^2 - iBB_x\right) \tag{30}$$

$$B_3 = \frac{3}{8}B^3 \tag{31}$$

where the reconstructed surface displacement is therefore :

$$\eta = \bar{\eta} + \frac{1}{2}\left[Be^{i\theta} + \frac{1}{2}(B^2 - iBB_x)Be^{2i\theta} + \frac{3}{8}B^3e^{3i\theta} + c.c\right] \tag{32}$$

5.2 An uniform grid

The number of points for reconstruction in both the longitudinal and transversal directions can be freely chosen. However, the reconstruction of the surface displacement requires a huge computational effort in time, limiting the number of points if we want to get the simulation ready in a reasonable time.

The numerical method by Lo & Mei [24] requires periodic boundary conditions in both horizontal directions. The computational domain has a length l in the longitudinal direction and a breadth b in the transversal direction. A uniform grid with N_l and N_b points in the physical and Fourier planes is employed. We construct an $N_l \times N_b$ grid of collocation points in the physical domain (x, y) :

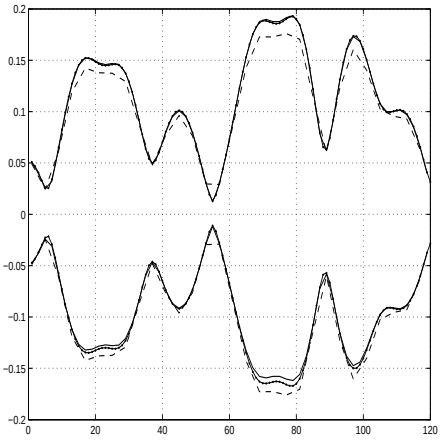

Figure 7: Surface envelope. Dashed curve : first order reconstruction, full curve : second order reconstruction and dotted curve : third order reconstruction.

$$(x_i, y_j) = \left(\frac{li}{N_l}, \frac{bj}{N_b}\right) \qquad \text{for } 0 \leq i \leq N_l \text{ and } 0 \leq j \leq N_b \tag{33}$$

The corresponding spectral components are

$$(k_{xp}, k_{yq}) = \left(\frac{2\pi p}{l}, \frac{2\pi q}{b}\right) \qquad \text{for } -\tfrac{1}{2}N_l \leq i \leq \tfrac{1}{2}N_l \text{ and } -\tfrac{1}{2}N_b \leq q \leq \tfrac{1}{2}N_b \tag{34}$$

The discretization of the Fourier space is $\triangle k_x = \frac{2\pi}{l}$ and $\triangle k_y = \frac{2\pi}{b}$. One can note that $(k_{xp}, k_{yq}) = (\triangle k_x p, \triangle k_y q)$.

5.3 Two types of spectra

We have been working with two types of initial spectra, the Gaussian spectrum and the JONSWAP spectrum. The spectrum is implemented in the program through the Fourier Transform of the first harmonic at $t = 0$. The relation between an envelope spectrum $F(\boldsymbol{K}, t)$ and the surface elevation η is :

$$\int F(\boldsymbol{K}, t) d\boldsymbol{K} = \overline{\eta^2} \tag{35}$$

where the wave vector is $\boldsymbol{k} = \boldsymbol{k_0} + k_0\boldsymbol{K}$ with $\boldsymbol{k_0} = (k_0, 0)$ and $\boldsymbol{K} = (K_x, K_y)$

1. The Gaussian shape spectrum

   For two horizontal dimensions, one can write the Gaussian shape spectrum as follows :

$$G(\boldsymbol{K}) = \frac{\bar{\eta^2}}{\pi\sigma_x\sigma_y}\exp\left[-\frac{1}{2}\left(\frac{K_x^2}{\sigma_x^2}+\frac{K_y^2}{\sigma_y^2}\right)\right] \tag{36}$$

From Equations 14 and 35, one can find the expression of the initialized Fourier transform of the first harmonic amplitude B :

$$\hat{B}(K_{pq},0) = \hat{B}_{pq}(0) = \sqrt{2G(K_{pq})\triangle K_x \triangle K_y}e^{i\theta_{pq}} \tag{37}$$

where θ_{mn} is the uniformly distributed phase on $[0, 2\pi]$ and $K_{pq} = (p\triangle K_x, q\triangle K_y)$.

For two horizontal dimensions, the initial Fourier amplitude is :

$$\hat{B}_{pq}(0) = \varepsilon\sqrt{\frac{\triangle K_x \triangle K_y}{2\pi\sigma_x\sigma_y}}\exp\left[-\frac{1}{4}\left(\frac{(p\triangle K_x)^2}{\sigma_x^2}+\frac{(q\triangle K_y)^2}{\sigma_y^2}\right)\right]e^{i\theta_{pq}} \tag{38}$$

where ε is the steepness equal to $k_0\sqrt{2\bar{\eta^2}}$.

Note that for one horizontal dimension, the initial Fourier amplitude reduces to :

$$\hat{B}_r(0) = \varepsilon\sqrt{\frac{\triangle K}{\sqrt{2\pi}\sigma_s}}\exp\left[-\left(\frac{r\triangle K}{2\sigma_s}\right)^2\right]e^{i\theta_r} \tag{39}$$

2. The directional spreading JONSWAP spectrum

   The JONSWAP project (see Hasselman et al. [28]) proposed an analytical expression for the spectrum of evolving surface gravity waves with increasing wind fetch. The sea state is characterized by a sharp spectral peak at a frequency ω_p that is decreasing with increasing fetch. For $\omega \leq \omega_p$, the JONSWAP spectrum has a steep forward face and for high frequency its tail follows the ω^{-5} power law. The analytical representation is

$$S(\omega) = \alpha g^2\omega^{-5}\exp\left[-\frac{5}{4}\left(\frac{\omega}{\omega_p}\right)^{-4}\right]\gamma^{\tau} \tag{40}$$

   This spectrum differs from the Pierson-Moskowitz (see [29]) spectrum through the presence of the peak enhancement factor γ^{τ} where γ is the ratio of the JONSWAP peak to the Pierson-Moskowitz peak. τ is given by

$$\tau = \exp[-(\omega-\omega_p)^2/2\sigma^2\omega_p^2] \tag{41}$$

$$\sigma = \begin{cases} \sigma_a & \text{for } \omega \leq \omega_p \\ \sigma_b & \text{for } \omega \geq \omega_p \end{cases} \tag{42}$$

The JONSWAP spectrum is thus described by five parameters $\omega_p, \alpha, \gamma, \sigma_a$ and σ_b where $\sigma_a = 0.07$ and $\sigma_b = 0.09$. α is called the Phillips constant.

In order to take the directional spreading of the waves into account it is convenient (see for example Onorato et al. [7]) to choose the directional spectrum as $F(\omega, \theta) = S(\omega)S_p(\theta)$ where $S_p(\theta)$ is taken to be

$$S_p(\theta) = \begin{cases} \frac{1}{\beta}\cos^2\left(\frac{\pi\theta}{2\beta}\right) & \text{if } -\beta \leq \theta \leq \beta \\ 0 & \text{else} \end{cases} \tag{43}$$

where $\theta = \arctan(k_y/k_x)$ with β a measure of the directional spreading.

To calculate the initial Fourier amplitude, we need to transform the frequency JONSWAP spectrum $F(\omega, \theta)$ into a wavenumber JONSWAP spectrum $F(\boldsymbol{k}) = S(k)S_p(\theta)$. With length and time scaled by k_p^{-1} and ω_p^{-1}, respectively, we get

$$S(k) = \frac{\alpha}{2k^4}\exp\left[-\frac{5}{4}k^{-2}\right]\gamma^{\tau} \tag{44}$$

$$\tau = \exp\left[-\frac{\left(\sqrt{k}-1\right)^2}{2\sigma_0}\right] \tag{45}$$

$$\sigma_0 = \begin{cases} \sigma_a & \text{for } k \leq 1 \\ \sigma_b & \text{for } k \geq 1 \end{cases} \tag{46}$$

We now use the wave vector $\boldsymbol{K}$ given by $\boldsymbol{k} = (1, 0) + \boldsymbol{K}$, and write $S_K(\boldsymbol{K}) = S(k)$. The initial Fourier amplitude is then given by

$$\hat{B}(K_{pq}, 0) = \hat{B}_{pq}(0) = \sqrt{S_K(K_{pq})S_p(\theta)\triangle K_x \triangle K_y}e^{i\theta_{pq}} \tag{47}$$

5.4 How some input parameters have been chosen

Some parameters as the type of the spectrum or the time simulation are very easy to set up. Note that the spectra have some internal parameters which must be chosen carefully. The question is even more tricky when we deal with the number of Fourier Modes, collocation points, steepness, ...

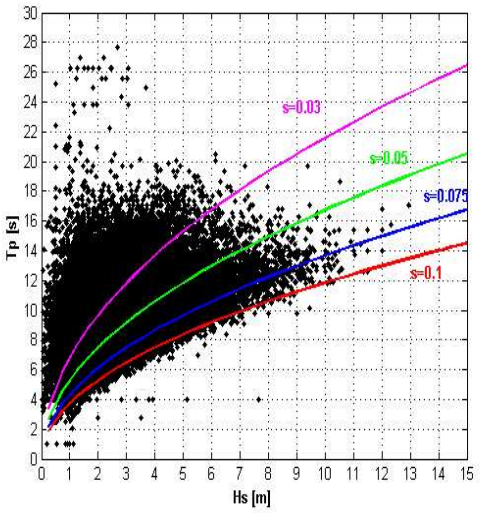

Figure 8: Scatter diagram from Haver et al. (2002) where the lines are of a constant steepness.

1. The steepness

   We remember the definition of the steepness parameter ε defined as $k_0 a$ where k_0 is a central wavenumber and a is a characteristic amplitude. In the following we take $k_0 \longrightarrow k_p$ and $a \longrightarrow (2\overline{\eta^2})^{1/2} = \sqrt{2}\sigma$ and denote this mean steepness by s thus

   $$s = k_p \sqrt{2\overline{\eta^2}} \tag{48}$$

   Haver et al. [30] made a scatter diagram (see Figure 8) of peak period T_p and significant wave height H_s with pooled data from the Northern North Sea (1973-2001) (nearly 70.000 data points). Curves of constant mean steepness (called s on the picture) are shown where $s = k_p \bar{a} = \frac{\sqrt{2}\pi^2}{g} \frac{H_s}{T_p^2}$. Here $\bar{a}$ is the rms value of the amplitude. Observing that the curve for steepness equal to 0.1 is on the border of the data points, we have decided to choose this value in most of our simulations.

2. The different parameters of the JONSWAP spectrum

   The JONSWAP spectrum is described by the set of Equations 40, 41 and 42. Equation 43 is used to take into account the directional spreading.
   The Philips constant α is chosen such that the steepness is equal to 0.1. The most probable values for some of the JONSWAP parameters are $\gamma = 3.3$, $\sigma_a = 0.07$

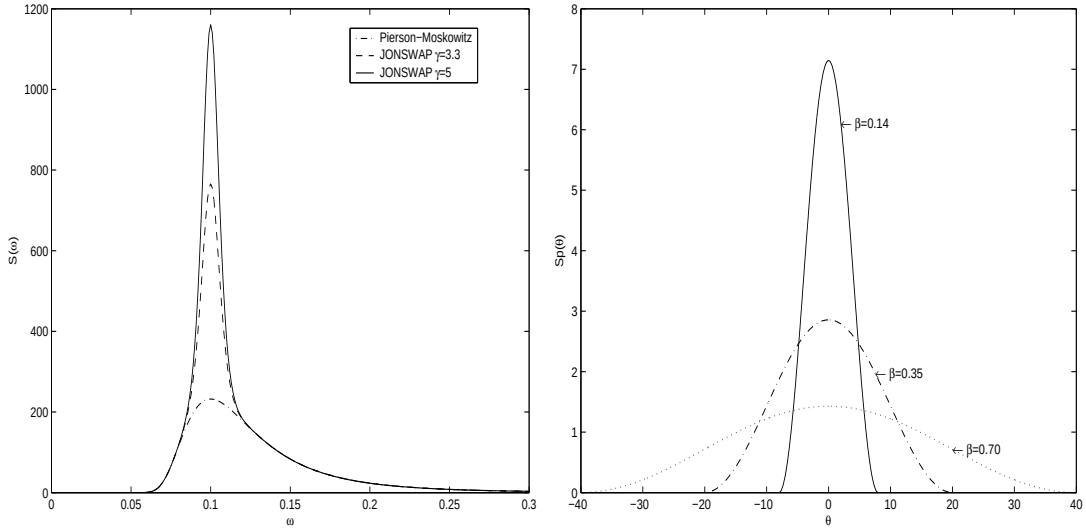

Figure 9: a) 2D spectra b) spreading function

and $\sigma_b = 0.09$ (see Torsethaugen and Haver [31]). However, Gunson and Magnusson [32] estimated some peak enhancements from measured data on Ekofisk (offshore platform in the North Sea) and WS Polarfront (Ocean Weather Station in the Norwegian Sea) during extreme storms. They have reported different γ up to 8.14. We shall use in the present thesis, the usual value $\gamma = 3.3$ reported by [31] and the value $\gamma = 5$ (see figure 9). It has been emphasized by [32] that the value $\gamma = 2$ is officially used by the Norwegian offshore industry.

Three different values of the spreading parameter β have been chosen (see Figure 9). In the Figure 10, one can see the effect of β on the waves. When β increases, the crests become shorter.

3. Number of waves and Fourier Modes

We define our ocean as a rectangular of size $N_x.\lambda_c$ and $N_y.\lambda_c$ where N_x and N_y are the number of characteristic wavelengths λ_c in the x and y direction. On all our simulations, we have been chosen $N_x = N_y = N$. Therefore, we have simulated a peace of ocean of size L^2 where $L = N\lambda_c$. For any given N we assign $2N$ Fourier modes. It's important to notice at we can increase the number of Fourier Modes as much as we want but it will also increase quite a lot the computation time and will not give any better results in our area of interests (for example, the k-spectrum). However, as Figure 11 shows, the size of N does really matter.

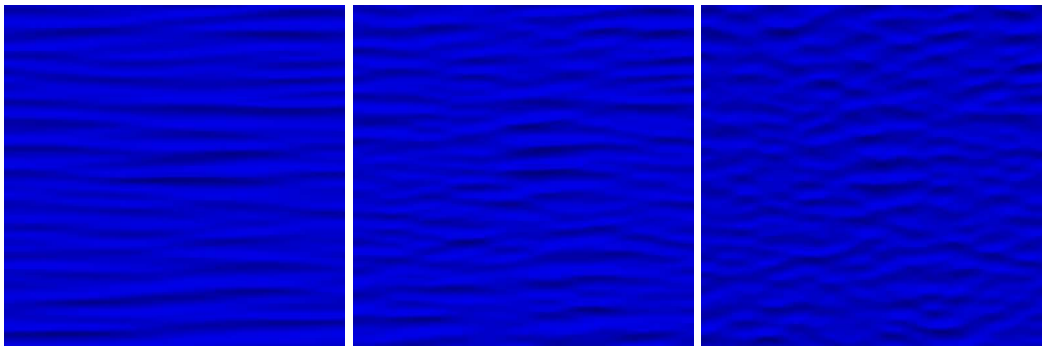

Figure 10: Surfaces of small sections of the computational domain for $\beta = 0.14$, $\beta = 0.35$ and $\beta = 0.7$.

The experience we got from our 1D simulations was the following :

- N must be higher than 32 in order to get a relatively good approximation of the spectrum.
- N equal to 64 and 128 gives qualitatively a good result.
- There is almost no difference between N equal to 128 and 256, concluding that it's a waste of time and data resources to choose N too high.

If we don't simulate an ocean large enough, we will lose information on the spectrum. As we shall see later, the evolution of the spectrum may play an important role concerning freak waves. It's obvious that the larger the simulated ocean is, the more data you get and the more accurate your statistical results will be. This is very important as we are interested in the freak waves which are rare events. It means that for a small N, we will need a lot of samples to get a good statistical result on the free surface distribution.

Even if we have performed some experiments with a Gaussian shaped spectrum, we spent most of our time on the JONSWAP spectrum. Results with a Gaussian spectrum can be found in [paper 1] where we verify the criterion of Alber (see [33], [34]) for a 2D simulation with the NLS Equation. However, we dont verify this criterion for a 3D simulation with the NLS. For the MNLS equation, we have found that the spectrum reaches a quasi-stationary state on the Benjamin-Feir timescale (see [35]).

5.5 Simulation cases

In the future, we will refer to the simulation cases :

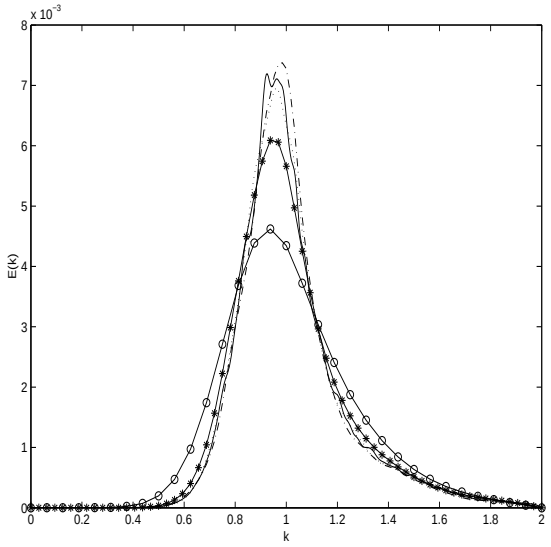

Figure 11: Simulated spectrum at a given time for different number of Fourier modes. $-\circ$ 32 FM, $-*$ 64 FM, $-\cdot$ 128 FM, $\cdot\cdot$ 256 FM, $-$ 512 FM

Case	γ	β
A	3.3	0.7
B	5	0.35
C	5	0.14
D	5	0.7
E	3.3	0.35
F	3.3	0.14

Table 1: Initial directional and JONSWAP parameters for simulation cases. All spectra are normalised to an initial steepness s= 0.1. $N_x = N_y = 128$. The cases A, B and C are the same as in [Paper 2] and [Paper 3].

6 Spectral evolution

6.1 Paper 1 : Evolution of a narrow-banded spectrum

Benjamin and Feir [35] showed that a uniform train of surface gravity waves is unstable to the well-known Benjamin-Feir (BF) instability. Alber and Saffman [33] and Alber [34], based on the Nonlinear Schrödinger (NLS) equation, demonstrated theoretically that for deep water waves, a nearly Gaussian random wave fields is stable only if spectral width σ_s is larger than twice the average steepness s.

$$\sigma_s > 2s \tag{49}$$

An extended work by Crawford et al. [36] gives some important results on the timescale where the spectral change should occur. According to their work, the spectrum should not change during the so-called BF timescale, $(s^2\omega_0)^{-1}$ but during the Hasselmann timescale, $(s^4\omega_0)^{-1}$ (see also Hasselmann [37]). Here ω_0 is the frequency associated to the wavenumber k_0 where the envelope spectrum is centred. Here $F(\boldsymbol{K}, x, t)$ is taken to have a Gaussian shape at the beginning of our simulations :

$$F_0(\boldsymbol{K}) = \frac{\bar{\eta^2}}{\pi\sigma_x\sigma_y} \exp\left[\frac{-1}{2}\left(\frac{K_x^2}{\sigma_x^2} + \frac{K_y^2}{\sigma_y^2}\right)\right] \tag{50}$$

In our paper, we have only investigated the case where $\sigma_s = \sigma_x = \sigma_y$ as it's a bit difficult to interpret Alber's result for the case of an asymmetric Gaussian spectrum. As Alber's result had never been verified with numerical simulations, we decided to do it using the NLS and MNLS equations developed by Dysthe [17] for both one and two horizontal dimensions.

1. NLS simulations

   In one horizontal dimension, we find that our simulations only approximately verify the Alber criterion for suppression of the modulational instability ($\sigma_s > 2s$). When $\sigma_s < 2s$, the spectrum widens symmetrically and reaches a quasi steady state on the BF timescale.

   In two horizontal dimensions, the NLS simulations do not support the Alber's result. Regardless the initial σ_s, we always observe that the spectrum widens. In the case $\sigma_s < 2s$, the spectrum flattens out to a plateau shape while in the other

case ($\sigma_s > 2\varepsilon$), the spectrum is particularly stretched in the directions $K_x = +\text{-}\sqrt{2}K_y$ of maximum BF growth rate

2. MNLS simulations

   The MNLS simulation does not support Alber's result neither in one nor in two horizontal dimensions.

   In one horizontal dimension, the spectrum evolves on the BF timescale, towards a quasi steady state which has the following characteristics :
   - an asymmetrical shape with a steepening of the low frequency side,
   - a widening of the high frequency side,
   - and therefore a downshift of the spectral peak.

   In two horizontal dimensions, the same phenomena are observed :
   - an asymmetric development,
   - downshift of the spectral peak k_p where $k_p < k_0$,
   - and an angular widening, mainly for $k > k_p$.

   For the angularly integrated spectrum, one can see a power-law behaviour $k^{-2.5}$ (that corresponds to ω^{-4} in the frequency spectrum) on the high frequency side $k > k_p$. Some steepening is observed on the low-frequency side. This occurs on the BF timescale.

6.2 Paper 2 & 3 : Evolution of a JONSWAP spectrum

Choosing different β in the angular distribution associated with the JONSWAP spectrum (see Onorato et al. [7]) in order to get simulations with short and long crested waves, we get approximately the same trend as already observed in [paper 1] for the Gaussian shape spectra. The spectra develop on the Benjamin-Feir timescale [35] and follow the $k^{-2.5}$ law for the integrated k-spectra even though it's not as clear as one can observed in [paper 1].

Spectral changes due to the modulational instability have been linked by theory and simulations to enhanced occurence of large freak waves (see [38], [39] and [40]. According to Skourup et. al [41], a wave is said to be freak if $A > 1.1H_s$ or $H > 2H_s$ where H is the waveheigth and H_s is the significant waveheigth equal to 4σ. For long crested waves, we demonstrate that the occurence of freak waves is significally increased while the main spectral change is taking place. This is in good agreement

with the experiment of Onorato et al. [42]. For short crested waves, however, the influence of spectral change seems rather insignificant.

7 Probabilities

In the following, we consider the random variate η which we take to be the surface elevation $\eta(\boldsymbol{x}, t)$. The mean is defined as the expected value of $\eta(\boldsymbol{x}, t)$ and can be written as

$$\mu = E[\eta(\boldsymbol{x}, t)] \tag{51}$$

where E denotes the expectation value of $\eta(\boldsymbol{x}, t)$. For deep water, which is assumed in this thesis, $\mu = 0$. The variance is therefore defined as

$$\sigma^2 = E\left[\eta^2(\boldsymbol{x}, t)\right] \tag{52}$$

The root-mean-square value of the process is called the standard deviation and is denoted σ.

We shall be concerned with the situation where the random variable η is statistically homogeneous. This implies that the autocorrelation function R is a function of the difference $\boldsymbol{x} = \boldsymbol{x_1} - \boldsymbol{x_2}$ only. Its definition is

$$R(\boldsymbol{x}, t) = E[\eta(\boldsymbol{x_1}, t)\eta(\boldsymbol{x_2}, t)] \tag{53}$$

The power spectrum $F(\boldsymbol{k})$ is defined as the spatial Fourier transform of $R(\boldsymbol{x}, t)$.

The cumulative probability function $P(x)$ is the probability that the signal $\eta(\boldsymbol{x}, t)$ takes a value less than or equal to x :

$$P(x) = Pr[\eta(\boldsymbol{x}, t) \leq x] \tag{54}$$

When $P(x)$ is a differentiable function, the probability density function (pdf) is

$$p(x) = \frac{dP}{dx} \tag{55}$$

where $p(x)$ is the probability density function. Thus $p(x)$ is the rate of change of $P(x)$. The area between two values a and b under the pdf $p(x)$ defines the probability that the results of an event will lie between the values a and b, that is

$$Pr(a \leq x(t) \leq b) = \int_a^b p(x)dx \tag{56}$$

The total probability of an event is unity thus

$$Pr(-\infty \leq x(t) \leq +\infty) = \int_{-\infty}^{+\infty} p(x)dx = 1 \tag{57}$$

The mean value and variance expressed in Equation 51 and 52, respectively, may be given in terms of the pdf $p(x)$ by

$$\mu = E[x(t)] = \int_{-\infty}^{+\infty} xp(x)dx \tag{58}$$

$$\sigma^2 = E\left[(x(t) - \mu)^2\right] = \int_{-\infty}^{+\infty} (x(t) - \mu)^2 p(x)dx \tag{59}$$

As an example, we choose the Gaussian distribution. The cumulative probability of a Gaussian distribution is given by :

$$P_G(x) = \frac{1}{\sigma\sqrt{2\pi}} \int_{-\infty}^{+x} \exp\left(-\frac{(y-\mu)^2}{2\sigma^2}\right) dy \tag{60}$$

and its probability density function is

$$p_G(x) = \frac{dP(x)}{dx} = \frac{1}{\sigma\sqrt{2\pi}} \exp\left(-\frac{(x-\mu)^2}{2\sigma^2}\right). \tag{61}$$

The Gaussian distribution is illustrated in Figure 12 with $\mu = 1.5$ and $\sigma = 1$.

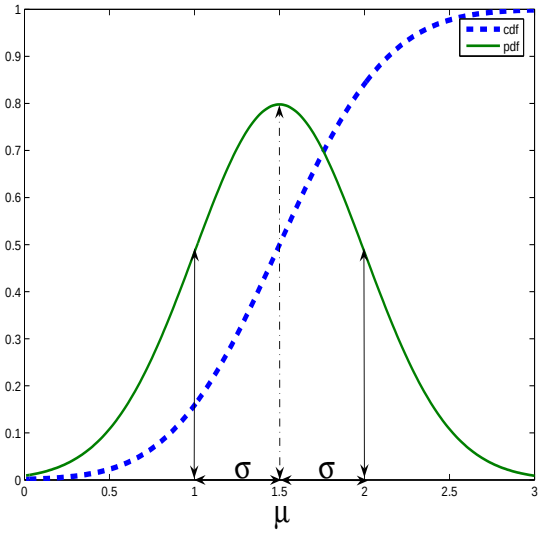

Figure 12: Gaussian Cumulative density function cdf and probability density function pdf

Other types of distributions are often used in water waves statistics. The most well-know is probably the Rayleigh distribution which can be expressed as

$$p_R(x) = \frac{2x}{\sigma^2} \exp\left(-\frac{x^2}{\sigma^2}\right) \tag{62}$$

$$P_R(x) = \exp\left(-\frac{x^2}{\sigma^2}\right) \tag{63}$$

Another type of distribution which is very common in the literature of ocean waves statistics is the Weibull distribution. It is written as

$$p_W(x) = \frac{\alpha x^{\alpha-1}}{\theta^\alpha} \exp\left[-\left(\frac{x}{\theta}\right)^\alpha\right] \qquad x \geq 0 \tag{64}$$

where α and θ are the shape and scale parameters, respectively. The Weibull distribution becomes a Rayleigh distribution when one sets $\alpha = 2$ and $\theta = \sigma$ (see the demonstration in Hu [43] for example).

The probability of exceedance P_e is defined as follow

$$P_e(x) = Pr(\eta(\boldsymbol{x}, t) > x) = 1 - P(x) \tag{65}$$

where $P(x)$ is the cumulative probability function.

The skewness $S(x)$ and kurtosis $K(x)$ are related to nonlinearities in a wave field. The skewness is a statistical measure of the vertical asymmetry of the sea surface exemplified by the sharp crests and rounded troughs. The kurtosis represents a degree of peakedness of the distribution when the normal distribution is taken as a reference.

The skewness of a random variable x with mean μ and variance σ^2 is defined as

$$S(x) = \frac{E[(x-\mu)^3]}{\sigma^3}. \tag{66}$$

If the skewness is negative (positive) the distribution is skewed to the left (right). Normally distributed random variables have a skewness of zero since the distribution is symmetrical around the mean.

The kurtosis of a random variable x with mean μ and variance σ^2 is defined as

$$K(x) = \frac{E[(x-\mu)^4]}{\sigma^4}. \tag{67}$$

Normally distributed random variables have a kurtosis of 3.

8 Distribution of the surface elevation, wave crest and wave height

Definitions of the wave crest and the wave height have already been given in a previous section. For a linear ocean, Gaussian properties of the surface elevation have been shown by Longuet-Higgins in 1952 [44] using the so-called Central Limit Theorem. Tayfun [45] considers a second order modification of Longuet-Higgins' results.
Longuet-Higgins [44] first introduced the Rayleigh distributions for prediction in wave amplitude in a narrow-banded random sea. Cartwright and Longuet-Higgins [46] modified the Rayleigh distribution to account for a more broad-banded random sea by including the spectral bandwith parameter. This broad-banded modification is not relevant in the present thesis as the assumption of a narrow-banded spectrum is made in the construction of the MNLS equations. Following Tayfun's assumptions [45], developments of second order wave crest distribution and surface elevation are developed.
Considering wave heights, several authors have proposed different models to improve the results of Longuet-Higgins [44]. Forristall [47] compared storm data from the Gulf of Mexico and found a good agreement with a Weibull distribution. Longuet-Higgins [48] and Naess [49] modified Longuet-Higgins previous result comparing with the storm data of Forristall. Mori and Yasuda [50] compared the validity of the Edgeworth-Rayleigh distribution with some experimental and field data.
More complete summaries of the wave crest and wave height models can be found in Prevosto and Forristall [51] and in Vinje [52]. Some of our results have already been published in [Paper 2] & [Paper 3].

8.1 Distribution of the surface elevation

In linear theory, Longuet-Higgins [44] showed that the complex amplitude B of the surface elevation η has a normal distribution under the following assumption

- The wave is the sum of a large number of small and statistically independent contributions.

The normal distribution of B is a direct consequence of the Central Limit Theorem. For an ocean of small bandwith, the surface elevation can be written as :

$$\eta = \frac{1}{2}(Be^{i\theta} + c.c.) + o(\epsilon) = a\cos(\theta + \psi) + o(\epsilon) \tag{68}$$

where a is the real amplitude, $\theta = \boldsymbol{k}\cdot\boldsymbol{x} - \omega t$ and ψ is a random phase. The wave number k is related to its wave frequency ω by the linear dispersion relation. In Figures13, 14 and 15 the Gaussian pdf normalized by the standard deviation σ is compared to the

first harmonic of some simulations of the MNLS equation with a JONSWAP initial spectrum.

A second order modification of Longuet-Higgins' result has been done by Tayfun [45]. In Paper 2, we have developed more suitable form for his results. Extension of Equation (68) to second order is the following :

$$\eta = \frac{1}{2}(Be^{i\theta} + B_2 e^{2i\theta} + c.c.) + o(\epsilon^2) \tag{69}$$

B_2 is the second harmonic equal to $\sigma B^2/2$. Using the following notations $x = a\cos(\theta+\psi)$ and $y = a\sin(\theta+\psi)$, we can write Equation (69) as :

$$\eta = x + \frac{\sigma}{2}(x^2 - y^2) + o(\epsilon^2) \tag{70}$$

Keeping the assumption of Longuet-Higgins that the complex amplitude B of the first harmonic is Gaussian implies that x and y, the real and imaginary parts are Gaussian as well with the joint distribution

$$\frac{1}{2\pi}\exp\left(-\frac{x^2+y^2}{2}\right) \tag{71}$$

Using Equation (70), one can find the cumulative distribution $P_{T1}(\eta)$ of the surface elevation η :

$$P_{T1}(\eta) = \frac{1}{2\pi\sigma^2}\int\int_{\eta\leq x+\frac{\sigma}{2}(x^2-y^2)} \exp\left(-\frac{x^2+y^2}{2}\right)dxdy \tag{72}$$

The probability distribution p_{T1} equal to $\frac{dP_{T1}}{d\eta}$ is given by

$$p_{T1}(\eta) = \frac{1}{\pi\sigma}\int_0^{+\infty} \exp\left[\frac{-x^2+(1-C)^2}{2\sigma^2}\right]\frac{dx}{C} \tag{73}$$

where $C = \sqrt{1+2\sigma\eta+x^2}$. $p_{T1}(\eta)$ was already found by Tayfun [45] in a more complicated form. Since the variance σ^2 is small, we can expand asymptotically the Equation (73) using the Laplace method. The leading term of the pdf is then

$$p_{T1}(\eta) \sim \frac{1-7\sigma^2/8}{\sqrt{2\pi(1+3G+2G^2)}}\exp\left(-\frac{G^2}{2\sigma^2}\right) \tag{74}$$

where $G = \sqrt{1+2\sigma\eta} - 1$.

In Figures13, 14 and 15 the Gaussian and Tayfun pdf normalized by the standard deviation σ are compared to the first and second harmonics of some simulations of the MNLS equation with a JONSWAP initial spectrum.

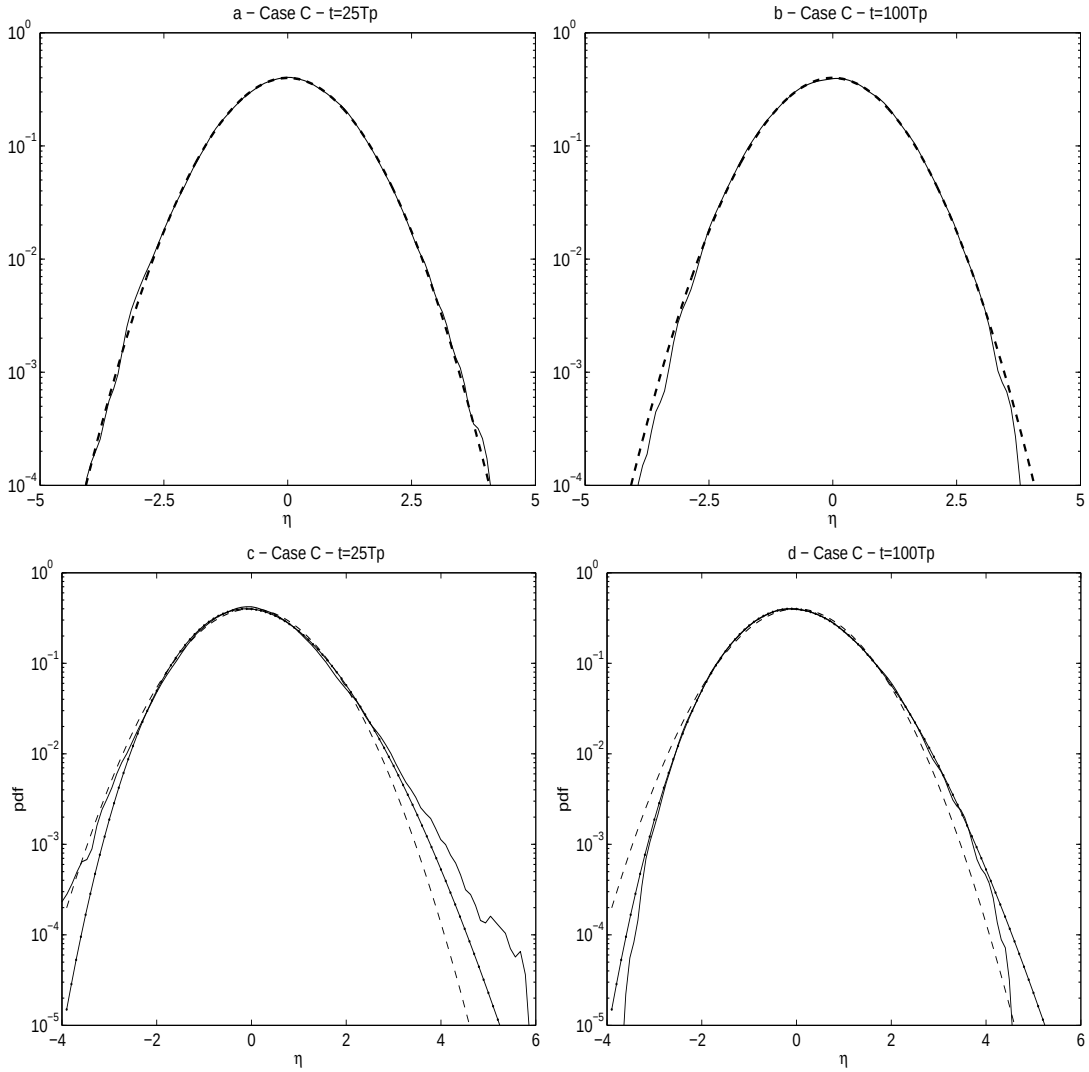

Figure 13: Dashed curve : Gaussian distribution, dotted curve : Tayfun distribution and full curve : simulation. a) and b) Simulated distributions of the first harmonic for the case C compared to a Gaussian distribution at two different times. c) and d) Simulated distributions of the first + second harmonics for the case C compared to the Gaussian and Tayfun distributions.

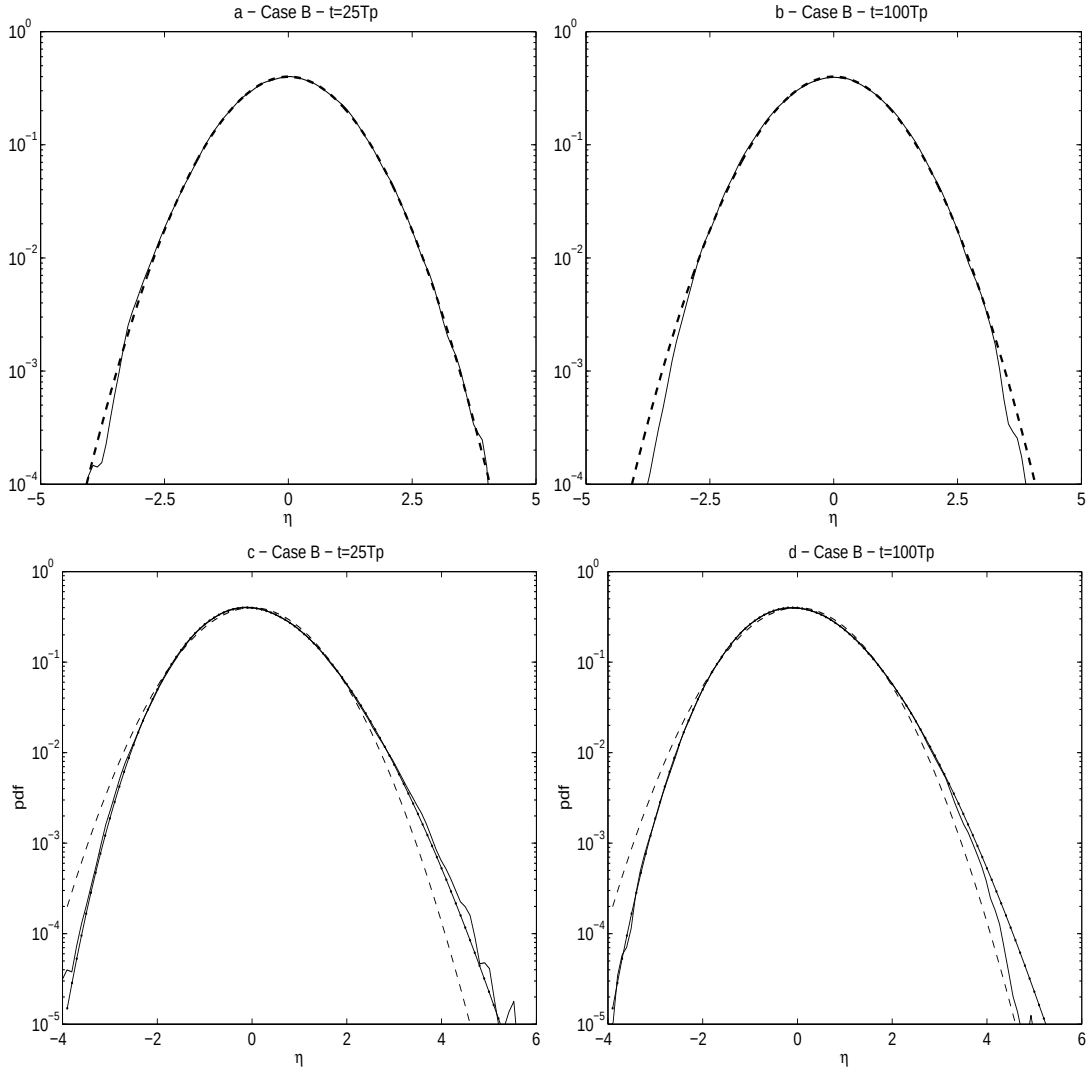

Figure 14: Same as Figure 13 but for the case B.

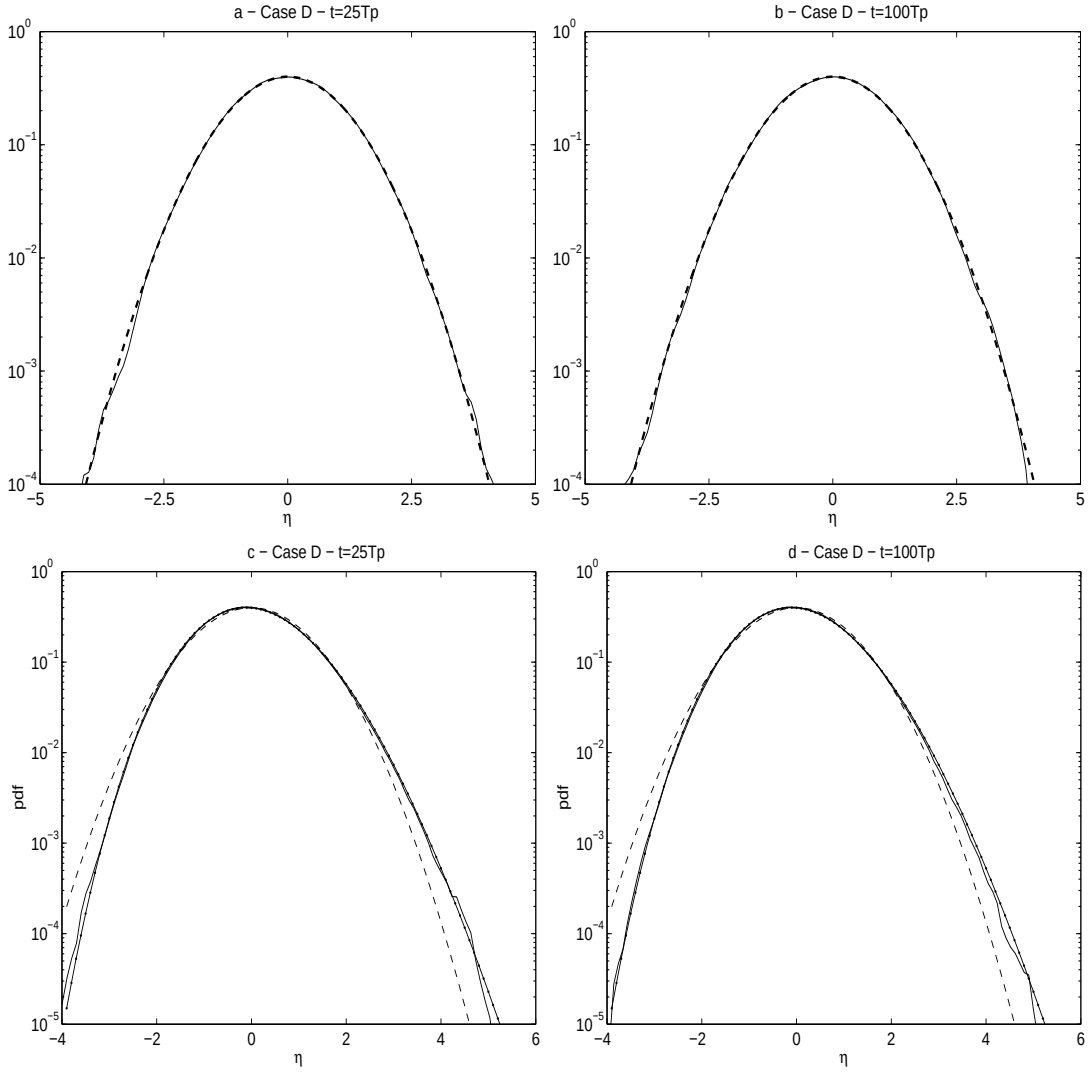

Figure 15: Same as Figure 13 but for the case D.

8.2 Distribution of the wave crests

We keep working under the assumption that the first harmonic complex amplitude is Gaussian distributed. Then Longuet-Higgins [44] showed that the first order surface envelope is Rayleigh distributed

$$p_R(a) = \frac{2a}{\bar{a^2}} \exp\left(-\frac{a^2}{\bar{a^2}}\right) \tag{75}$$

where $\bar{a^2} = 2\bar{\eta^2} = 2\sigma^2 = 2m_0$. [Paper 2] gives the reason why the distribution of wave crests can be associated to the upper surface envelope. The explanation comes from a property of invariance of the MNLS equations with respect to a phase shift. We get the following expressions for the first and second order envelopes of the wave field :

$$\begin{cases} a = |B| & \text{first order envelope} \\ A = a + \frac{\sigma}{2}a^2 & \text{second order upper envelope} \end{cases} \tag{76}$$

Tayfun [45] takes second offer effects into account, still assuming that a is Rayleigh distributed. Due to the Equation (76), we get the following relationship between the pdf of the first order envelope $p_R(a)$ and the pdf of the second order envelope $p_{T2}(A)$

$$p_R(a)da = p_{T2}(A)dA \tag{77}$$

Using the relation $a = \sqrt{1 + 2\sigma A} - 1$, one get easily $\frac{da}{dA} = \frac{\sigma}{\sqrt{(1+2\sigma A)}}$. The pdf of the second order envelope is finally obtained :

$$p_{T2}(A) = \frac{1}{\sigma}\left(1 - \frac{1}{\sqrt{2\sigma A + 1}}\right) \exp\left[-\frac{1}{\sigma^2}(\sigma A + 1 - \sqrt{2\sigma A + 1}\right] \tag{78}$$

Similar work has been done by Tung and Huang [53] and was corrected by Tucker [54] as Warren et al. [55] pointed out.
Another possibility of deriving a pdf by taking into account the second order contributions is to assume that the Equation (75), with A substituted for a and $\bar{A^2}$ for $\bar{a^2}$ Here $\bar{A^2} \simeq \bar{a^2} + \bar{a^3} = 2\sigma^2 + \frac{3\sqrt{\pi}\sigma^3}{2}$ where we have used Equation (75) as follows

$$\bar{a^3} = \int_0^\infty a^3 p_R(a)da = \frac{3\sqrt{\pi}\sigma^3}{2} \tag{79}$$

We have called this, the Modified Rayleigh distribution p_{MR} . Here, we note that the second order envelope we have discussed so far is only valid for the upper envelope. The lower envelope to second order is $A = a - \frac{\sigma}{2}a^2$. It is easy to derive p_{T2} and p_{MR} associated with the lower envelope. The two distributions are quite closed for $x < 3$ but even here the Tayfun distribution gives the best fit to our simulated data. For

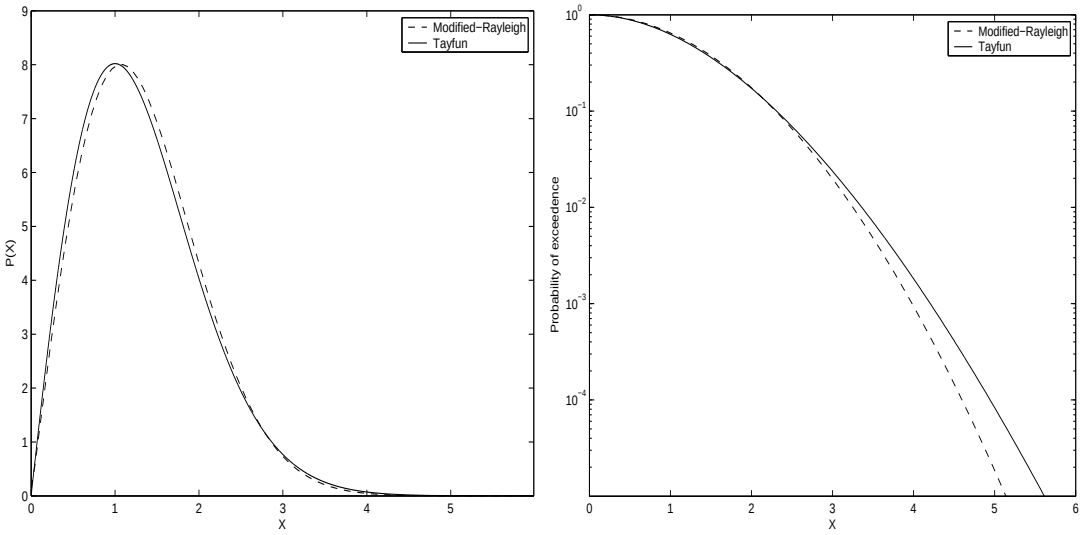

Figure 16: a) Pdf of the Tayfun and Modified-Rayleigh distributions for second order. b) Probability of exceedance of the Tayfun and Modified-Rayleigh distributions

lager waves ($x > 3$), the difference between the two distributions becomes much more significant, as seen in the exceedance plot (see figure 16).

Figures 17 and 18 show that the Rayleigh and Tayfun distributions fit well with our simulations. For the first order, $\bar{a^2} = s^2 = 0.01$ where s is the steepness set to 0.1 in all our simulations. We compute $\bar{a^2}$ at any time of our simulations and find $0,0100036$ after averaging over space. At second order, $\bar{A}^2 = 0.01132$ for the upper envelope and 0.00867 for the lower envelope. We find respectively with our simulations 0.001126 and 0.00865.

Various authors as pointed out by Krunic and Winterstein [56] have used the Weibull distribution p_W (see Equation 64) to study the wave crest statistics. They claim that the Weibull distribution doesnt approximate good enough the distribution of wave crests and build another distribution based on the Weibull distribution called the Noisy-Weibull distribution and named p_{NW} :

$$p_{NW}(x) = \left[1 + \frac{1}{2}\left(\frac{\bar{\alpha}\sigma}{\bar{\theta}}\right)^2 \left(\frac{x}{\bar{\theta}}\right)^{2\bar{\alpha}-2}\right] \exp\left[-\left(\frac{x}{\bar{\theta}}\right)^{\bar{\alpha}}\right] \tag{80}$$

where $\bar{\theta} = k_1\theta^{k_2}$ and $\bar{\alpha} = \alpha/k_2$ with k_1 and k_2 numerical values from data.

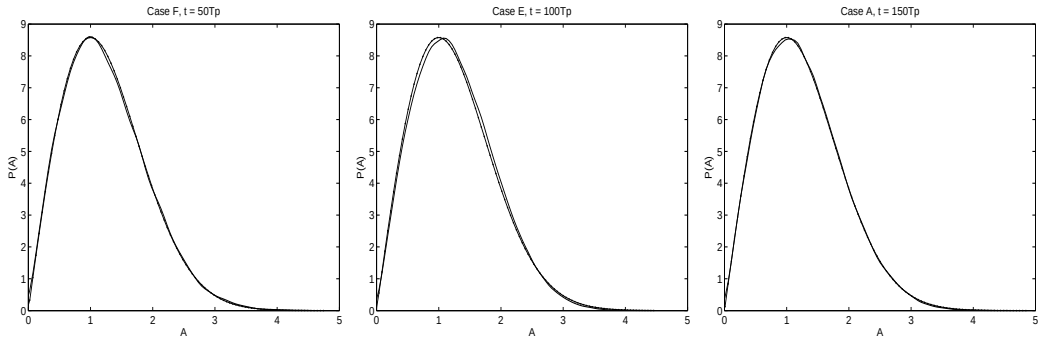

Figure 17: Dotted curve : Rayleigh distribution and full curve : simulation. First order surface envelope compared with the Rayleigh distribution for the cases A, E and F at different times

8.3 Distribution of the wave height

In linear theory, for extremely narrow band waves,the wave height H is twice the amplitude and is therefore Rayleigh distributed :

$$p_R(h) = \frac{2h}{\bar{h^2}} \exp\left(-\frac{h^2}{\bar{h^2}}\right) \tag{81}$$

where $\bar{h^2} = 4\bar{a^2} = 8m_0$. Forristall [47] showed that this distribution failed to fit storm data from the Gulf of Mexico. He showed that a Weibull distribution reduced to the form $\frac{\alpha x^{\alpha-1}}{\beta} \exp(-x^\alpha/\beta)$ with parameters $\alpha = 2.126$ and $\theta = 8.42$ gives good agreement with his storm data. Longuet-Higgins [48] showed that choosing $\bar{h} = 2.62\sqrt{2m_0}$ in Equation (81) gives equally good fit to the storm data from the Gulf of Mexico as that of Forristall's empirical Weibull distribution. Longuet-Higgins pointed out that his empirical Rayleigh distribution has only one estimated parameter instead of two for Forristall. Naess [49] uses another approach to calculate the pdf of the wave heights. Like Longuet-Higgins [48], he assumes that the process is Gaussian. He arrives at the result for the exceedance probability

$$P_N(H > h) = \exp\left(-\frac{h^2}{4m_0(1-r')}\right) \tag{82}$$

where $r' = R(T/2)/m_0$ where $R(\tau)$ is the autocorrelation function of the process and T is chosen such as $R'(T) = 0.$.

Looking at the rms value $\bar{h}$ of the wave height H, we can compute Forristall, Longuet-Higgins and Naess distributions given above. In Longuet-Higgins paper, we find $\bar{h} \simeq 2.62\sqrt{m_0}$. Naess calculates the autocorrelation function for the JONSWAP spectrum for values of peakedness parameter γ in the range 1-7. For $\gamma = 3.3$, we get

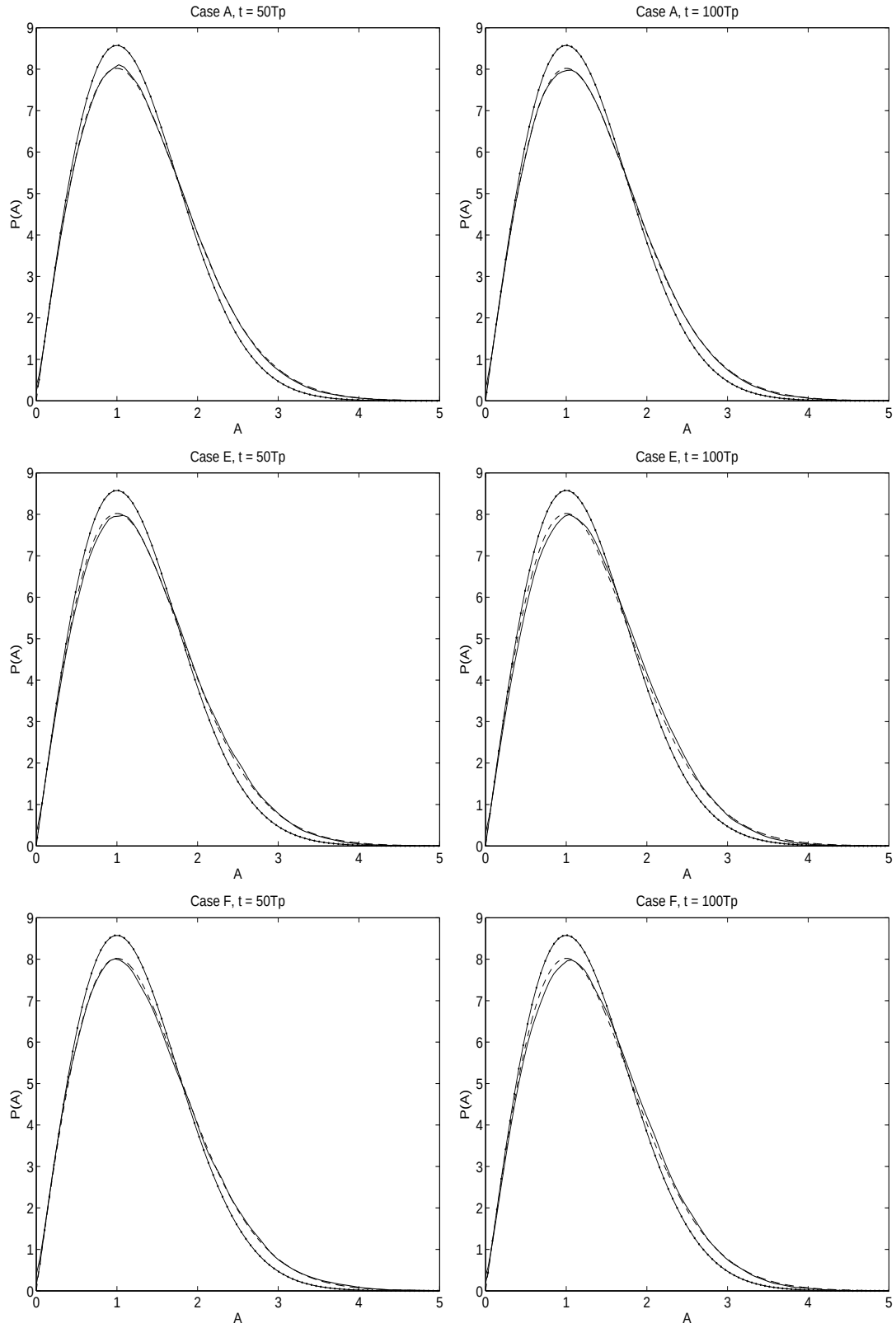

Figure 18: Dashed curve : Equation 78, dotted curve : Rayleigh distribution and full curve : simulation. Second order surface envelope compared with the Rayleigh and Tayfun distributions for the cases A, E and F at 50 and 100 Tp

$r' \simeq -0.73$ which gives $\bar{h} \simeq 2.63\sqrt{m_0}$. Forristall gives an empirical relation between the average largest third of the waves, $H_{1/3}$ and the rms value of the surface elevation such as $H_{1/3} \simeq 3.77\sqrt{m_0}$. From the Rayleigh distribution, one can get an expression of $H_{1/3}$ as a function of $\bar{h}$. We find $H_{1/3} \simeq 1.416\bar{h}$. Combining the last two expressions yields $\bar{h} = 2.66\sqrt{m_0}$.

In a two-dimensional wave record, as a time series from a buoy or a laser instrument, it's easy to define the wave heights. It turns out that it becomes much more difficult in three dimensions. We describe here two possible options for extracting the waveheigths in a three dimensional data base.

1. Method 1 using the surface elevation. Using the reconstructed free surface, at a given time, we can extract, along the main wave direction x for a given y, the waveheigths. This way we can compute the successive minima and maxima. Then we repeat the procedure for different y and t.

2. Method 2 using the upper and lower envelopes (respectively A_u and A_l. If all waves had a period T_p, the waveheigth as measured at a given location would be $h = A_u(t) - A_l(t + T_p/2)$. From equation (76), we can deduce $h = a(t) + a(t + T_p/2) + o(\varepsilon^2)$. The advantage of this method is that we can have all the waveheigths at a particular time but on the other hand, all waves don't have the exact period T_p.

Figures 19, 20 and 21 compare the two methods for the cases A, E and F with the Rayleigh, Naess and Edgeworth-Rayleigh distributions (see [50]). A first result is that Method 1 doesn't fit with any distributions. The same occurs for the long crested waves (case F) using the Method 2. However, fairly good agreement between the Naess distribution and the Case E can be observed for Method 2. For the short crested waves (case A), very good agreement between the Naess distribution and our simulations has been found. Method 1 failed to catch the higher waves of the distribution while Method 2 managed to do it for a directional spreading large enough.

8.4 Probability of exceedance for the wave crests

Using the Rayleigh and Tayfun probability density functions (see Equations 75 and 78), we find the respective probabilities of exceedance for the crest height A to be given as

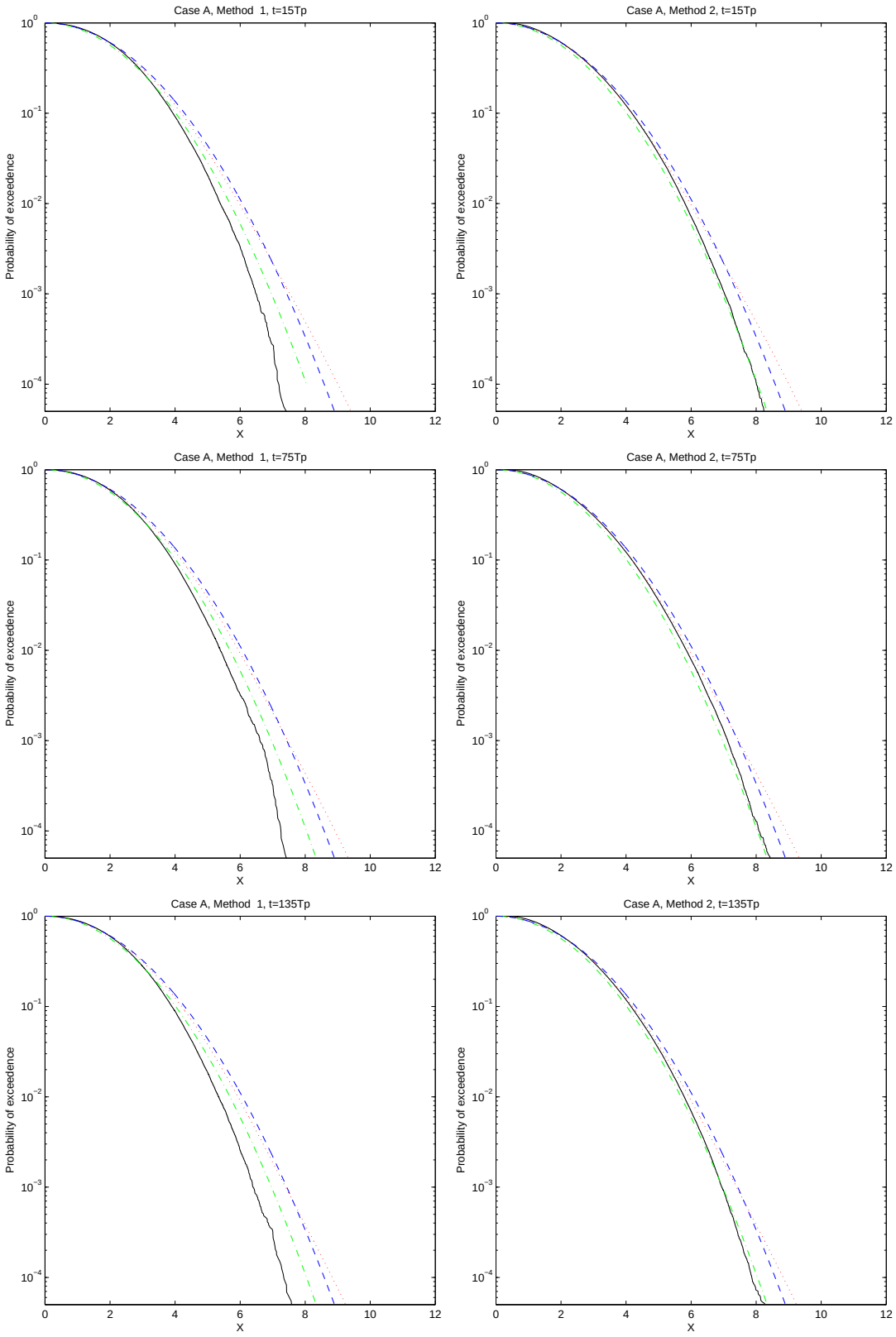

Figure 19: Probability of exceedance for the wave height. Case A, Methods 1 and 2. Full curve : simulation. Dash-dotted curve : Naess distribution. Dashed curve : Rayleigh distribution. Dotted curve : Edgeworth-Rayleigh distribution.

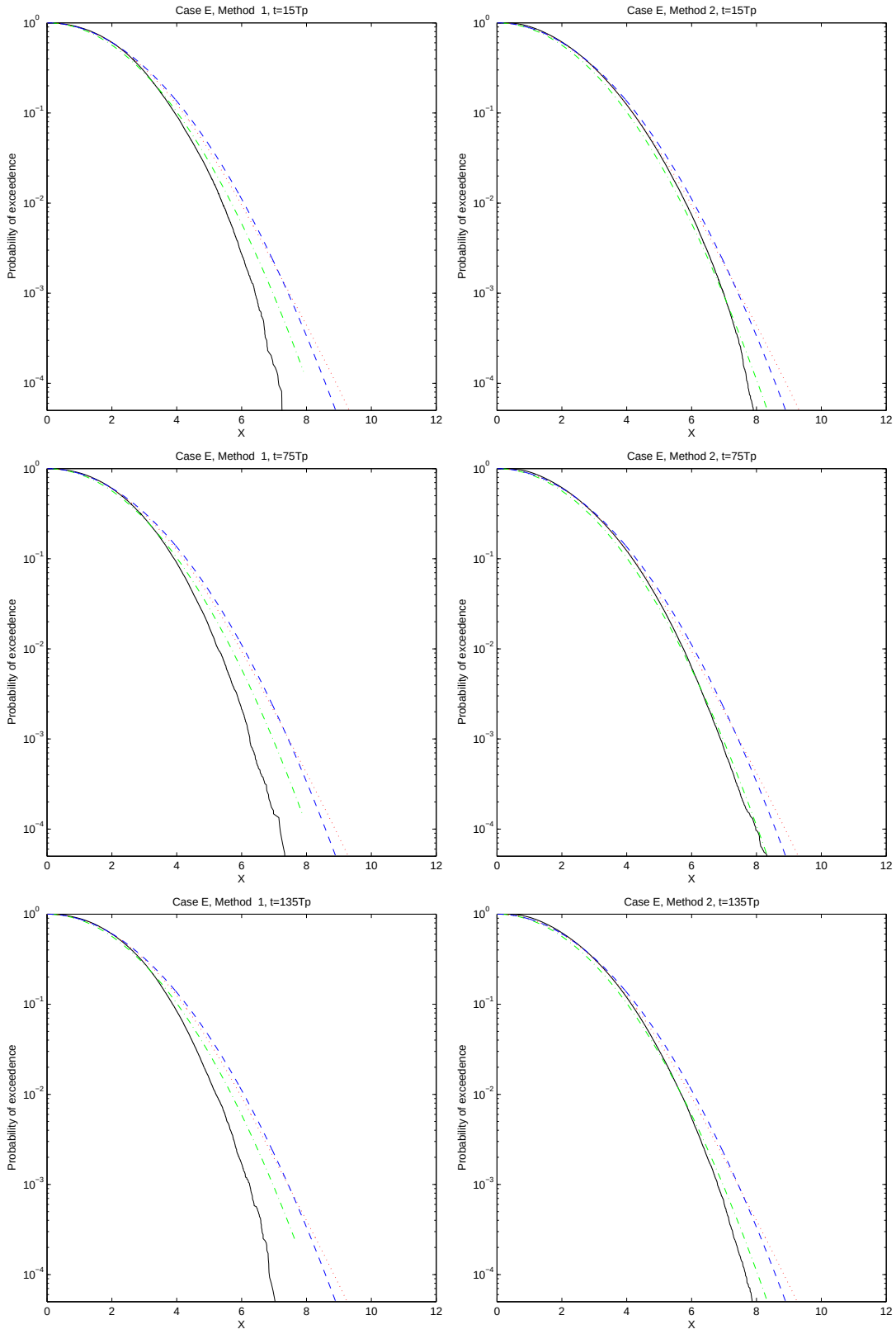

Figure 20: Same as Figure 19 for the case E.

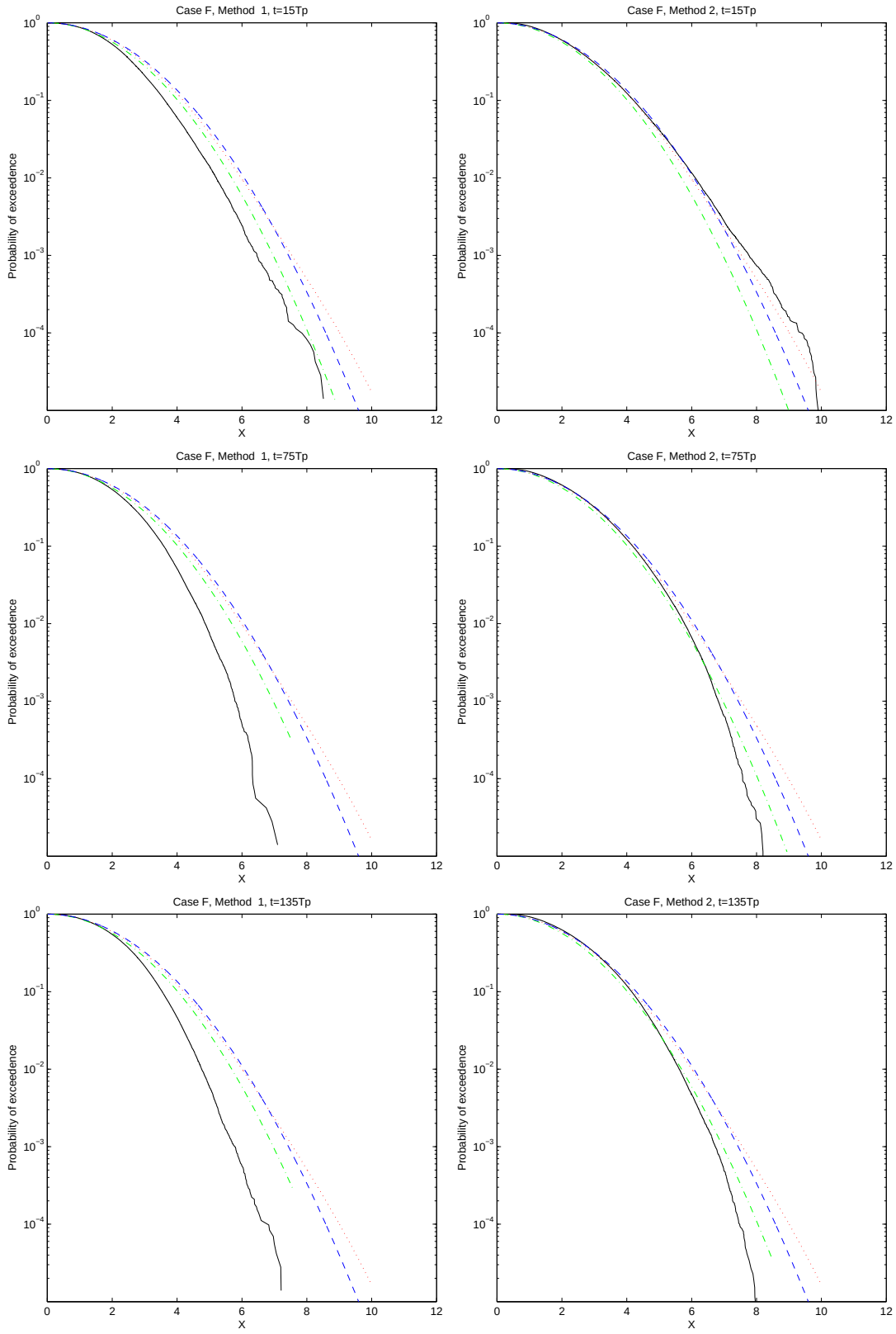

Figure 21: Same as Figure 19 for the case F.

$$Pr^R(A > x) = \exp\left(-\frac{x^2}{2}\right) \tag{83}$$

$$Pr^T(A > x) = \exp\left[-\frac{1}{\sigma^2}(\sigma x + 1 - \sqrt{2\sigma x + 1})\right] \tag{84}$$

Equation (84) was also derived by Tucker [54]. Developing of $\sqrt{1+x}$ for small x, Kriebel and Dawson [57] found an approximation of Equation (84) up to third order in x :

$$Pr^T \simeq \exp - \left[0.5(x^2 - \sigma x^3)\right] \tag{85}$$

Note that since the third order development of B includes some derivatives, it is not possible to find an exact expression for the third order envelope distribution.

9 Extreme value analysis

In a large number of situations, we are interested in only one part of the distribution. When one wants to study some dramatical situation (rogue waves for instance), we focus on the distribution of the very high values. In the present thesis, one of our main interest is the study of freak waves. Therefore we need to look closer at the extreme value theory. Leder *et al.* [58] give a brief historical review of the theory of extremes. According to Gumbel [59], the first principles of this theory had been exposed by Bernoulli in 1709. Fisher and Tippet [60] gave an important step forward by introducing the stability principle from which Gumbel derived one form of the distribution of extremes. Pioneer work in the analysis of extreme values of a stochastic process had also been done by Rice [61]. He derived an important expression on the mean number of level-crossings of a given level which is named the Rice formula. Extension of his work for a Gaussian process of higher dimensions has been given by Piterbarg [62]. It states that the asymptotic cumulative distribution of the maxima of a Gaussian ocean containing N waves has a Gumbel law when N goes to infinity.

9.1 Generalized Extreme Value Distribution

Let $F(x)$ be the probability that a sample of random variables has a value lower or equal to x. Assume that $F(x)$ can be written as

$$F(x) = 1 - e^{-h(x)} \tag{86}$$

where $h(x)$ increases monotonously with x and has no upper limit. A distribution with this property is said to be of the exponential type. The probability that the largest out of n random samples has a value $\leq x$ is $F^n(x)$. For a distribution with the property 86 one can show that asymptotically when $n \longrightarrow \infty$

$$F^n(x) \sim \exp\left(-\exp[-\alpha_n(x - u_n)]\right) \tag{87}$$

where the right hand side is the Gumbel distribution with parameters α_n and u_n. For the case that $F(x)$ is a Rayleigh distribution we have $\alpha_n = u_n = \sqrt{2 \ln n}$.
Generally the mean value and variance of the distribution 87 are

$$\bar{x_n} = u_n + \frac{\gamma}{\alpha_n} \tag{88}$$

$$\sigma_n^2 = \frac{\pi^2}{6\alpha_n^2} \tag{89}$$

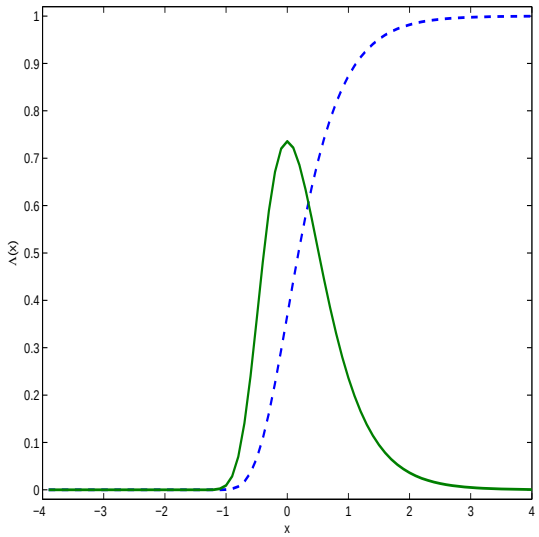

Figure 22: Cumulative (dashed curve) and probability (full curve) density functions of the Gumbel distribution $\Lambda(2x)$

where γ is the Euler-Macheroni constant.
A normalized version of the Gumbel distribution, $\Lambda(x) = \exp(-\exp(-x))$ is shown in Figure 22.

9.2 The Rice formula

9.2.1 Its definition and a non-rigorous proof

We say that a process $X(t)$ has an upcrossing of the level a at t_0 if

$$X(t_0) = a \qquad \text{and } \dot{X}(t_0) > 0 \tag{90}$$

The Rice formula states that the expected number of upcrossing per time unit, that is, the upcrossing frequency, may be expressed as :

$$\nu_X^+(a) = \int_0^\infty \dot{x} f_{X\dot{X}}(a, \dot{x}) d\dot{x} \tag{91}$$

where $f_{X\dot{X}}$ is the joint distribution of X and $\dot{X}$. A non-rigorous proof can be made by assumptions about the smoothness of the process. Then, the path of $X(t)$ can be approximated by a Taylor expansion $X(t) \simeq X(t_0) + \dot{X}(t_0)(t - t_0)$. The probability ϖ to have one crossing in a interval Δt is

$$\varpi = Pr\left(\{X(t) < a\} \cap \{(X(t) + \dot{X}(t)\Delta t) > a\}\right) \tag{92}$$

$$\varpi = \int_{\dot{x}=0}^{\infty} \int_{a-\dot{x}\Delta t}^{a} f_{X\dot{X}}(x, \dot{x}) dx d\dot{x} \tag{93}$$

$$\varpi \simeq \Delta t \int_{\dot{x}=0}^{\infty} \dot{x}\Delta t f_{X\dot{X}}(x, \dot{x}) d\dot{x} \tag{94}$$

Since $\varpi = \nu_X^+(a)\Delta t$, Equation 91 follows.

9.2.2 Application to Gaussian Process

Let X be a smooth Gaussian process. Then also $\dot{X}$ is Gaussian, and X and $\dot{X}$ are independant. The pdf of a Gaussian distribution has been given by the Equation (61). The joint distribution is then

$$f_{X\dot{X}}(x, \dot{x}) = \frac{1}{\sqrt{2\pi}\sigma_X} \exp\left(-\frac{x^2}{2\sigma_X^2}\right) \frac{1}{\sqrt{2\pi}\sigma_{\dot{X}}} \exp\left(-\frac{\dot{x}^2}{2\sigma_{\dot{X}}^2}\right) \tag{95}$$

where σ_X and $\sigma_{\dot{X}}$ are the standard deviations corresponding to X and $\dot{X}$ respectively. Then, we obtain

$$\nu_X^+(a) = \frac{1}{2\pi} \frac{\sigma_{\dot{X}}}{\sigma_X} \exp\left(-\frac{a^2}{2\sigma_X^2}\right) \tag{96}$$

Having in mind that the general definition of a moment of order n is $m_n = \int_0^\infty \omega^n S(\omega) d\omega$ where $S(\omega)$ is the frequency spectrum, it's easy to get the mean zero upcrossing frequency. $\sigma_X^2 = m_0$ and $\sigma_{\dot{X}}^2 = m_2$ so $\nu_X^+(0) = \frac{1}{2\pi}\sqrt{\frac{m_2}{m_0}}$. The mean zero upcrossing period is equal to $\frac{1}{\nu_X^+(0)}$ which is usually denoted T_z.

9.3 The Piterbarg's Theorem

The Pitebarg's theorem [62] gives the expressions for the asymptotical distributions for homogeneous Gaussian in fields in $\mathbb{R}^n$. In the present thesis, we are only interesting in the cases $n = 1$ and $n = 2$ (the cases of a times series and a random surface respectively).
We begin with a somehow technical approach of the theorem. We start with an ocean Gaussian field in $\mathbb{R}^n$ and define a system of closed subsets T_k, $k = 1, \cdots, n$ with volumes $\tau_k = V(T_k)$. For the cases $n = 1$ and $n = 2$, the volumes reduce to a line and a surface, respectively. The field is required to satisfy rather strong regularity

conditions, like being three times differentiable. We denote x_m the maximum of the ocean Gaussian field. In $\mathbb{R}^1$, Pitebarg's theorem gives

$$P^{1D}r(x_m \leq a) \sim \exp\left(-N\exp\left(-\frac{a^2}{2\sigma^2}\right)\right), \tag{97}$$

where N is the length of the time series divided by T_z and σ is the standard deviation. It's interesting to note that the correct N used in the previous equation is not necessarily the natural number of waves. We therefore refer to N as a the number of "waves" (with brackets).

In two dimensions, the analogue of the mean zero-crossing period turns out to be an area connected with an average wave. The size of one "wave" as defined by Piterbarg is $S' = \lambda_0\lambda_c/\sqrt{2\pi}$ where λ_0 and λ_c are the mean wave length and the mean crest length of the field, respectively, and are defined as follow :

$$\lambda_0 = \frac{2\pi}{sqrt\langle k_x^2\rangle}, \lambda_c = \frac{2\pi}{sqrt\langle k_y^2\rangle} \tag{98}$$

where

$$\langle k_{x,y}^2\rangle = \frac{\int k_{x,y}^2 F(k_x,k_y)dk_xdk_y}{\int F(k_x,k_y)dk_xdk_y} \tag{99}$$

where $F(k_x,k_y)$ is the wave spectrum. The size of our computational domain, S, is $N_xN_y\lambda_p^2$ where N_x and N_y are the number of Fourier modes. Thus the number of "waves", N, is S/S'. The Piterbarg theorem states the asymptotic result

$$P^{2D}r(x_m \leq a) \sim \exp\left[-\frac{a}{h_N\sigma^2}\exp\left(-\frac{1}{2}\left(\frac{a}{\sigma}\right)^2 - h_N^2\right)\right] \tag{100}$$

where h_N is the solution of the equation $Nh\exp(-h^2/2) = 1$ that is $h_N = \sqrt{2\ln N + \ln(2\ln N + \ln(2\ln N + \cdots))}$. When $N \longrightarrow \infty$, the distribution P_2 tends to a Gumbel distribution. The result 100 can be extended to the second order surface by using the result of the Equation (76) and assuming that the first order surface is Gaussian. If we denote η_1 the elevation of the first order surface, we then find that the second order maximum η_m is given by $\eta_m = \eta_{1m} + \frac{\sigma_X}{2}\eta_{1m}^2$. The asymptotic distribution of the second order surface is the obtained from (100) by applying the transformation $x \rightarrow \frac{1}{\sigma_X}(\sqrt{1+2\sigma x} - 1)$. We shall call this distribution the Piterbarg-Tayfun distribution. The asymptotic Gumbel limit of the Piterbarg-Tayfun distribution, $\Lambda_{PT}(x)$, is

$$\Lambda_{PT}(x) = \exp\left[-\exp\left(-\frac{h_N - 1/h_N}{1+\sigma h_N}(x - (h_N + \frac{\sigma}{2}h_N^2))\right)\right] \tag{101}$$

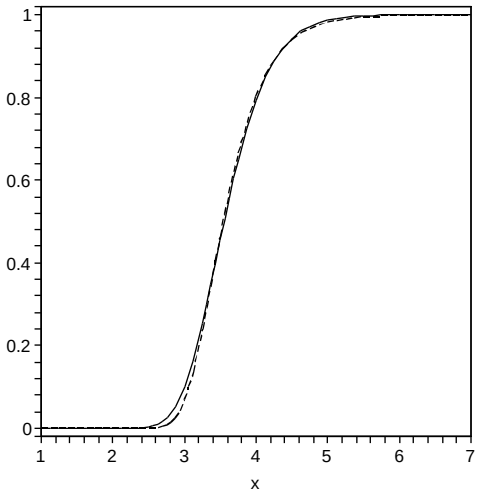

Figure 23: The Piterbarg-Tayfun distribution (full curve) and its asymptotic Gumbel limit (dotted curve) for $N = 40$ and $\sigma = 0.071$.

Figure 23 shows that the Piterbarg-Tayfun distribution and its asymptotic Gumbel limit match almost perfectly.

The corresponding expectation value of η_m is then

$$E(\eta_m) \simeq h_N + \frac{\sigma}{2} h_N^2 + \frac{\gamma(1 + \sigma h_N)}{h_N - 1/h_N} \tag{102}$$

where γ is the Euler-Macheroni constant equal to 0.5772. In Figure 24, we compare the result obtained in 102 with the simulations for the case A. A good agreement between the theory and our simulations is observed.

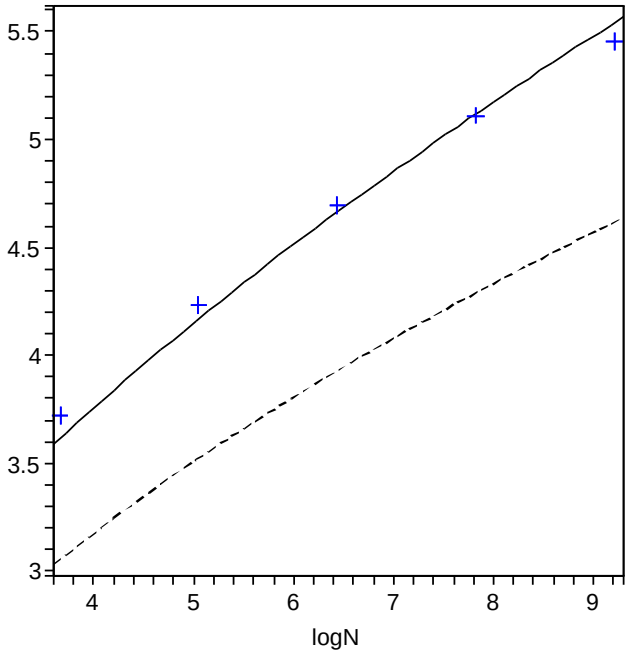

Figure 24: The average largest surface elevation of scenes containing N waves. Full curve : Expected value of η_m according to the asymptotic Gumbel limit of the Piterbarg-Tayfun distribution. Dashed curve : Expected value of η_m according to the Gaussian distribution. Crosses : Simulations. The sizes of the scenes in term of the number of "waves" go from 40 to 10.000.

10 Concluding remarks

Numerical simulations of the evolution of gravity wave spectra of fairly narrow bandwith have been performed.
In two dimensions, the NLS equation support the Alber's result. When it comes to three dimensions, it's no longer valid. Our simulations using the MNLS equation do not support Alber's result neither two or three dimensions.
We have noticed that our spectra evolve on the Benjamin-Feir timescale $(s^2\omega_0)^{-1}$. In two dimensions, the spectrum reaches a quasi steady state. In three dimensions, it can be seen that the spectrum follow a power-law behaviour $k^{-2.5}$.
Using a truncated initial JONSWAP spectrum (with different peak enhancements and spreading angles), we have seen that the evolution of such a spectrum is linked to the frequency of extreme waves for long-crested waves. Such a relation has not been observed for short crested waves.
The probability distributions of surface elevation and crest height are seen to fit the theoretical distributions found by Tayfun. Very good agreement between the theory and our simulations has been found up to 4 standard deviations.
The wave height distributions only fit the distribution found by Naess for the long crested simulations. This result is to take cautiously due to the ways we calculate the wave height.
We have also verified that our simulations support surprisingly well the result established by Piterbarg about the distribution of extremes.

References

[1] World Meteorological Organization (1998). Guide to wave-analysis and forecasting. WNO-No 702. Ch1, 4.

[2] Kharif, C., Pelinovsky, E. & Talipova, T. (2000) Formation de vagues géantes en eau peu profonde. C.R. Acad. Sci. Paris, t. 328, Série II b, p. 801-807. Mécanique des fluides.

[3] Lavrenov, I.V. (1998) The wave energy concentration at the Agulhas current of South Africa. Natural Hazards 17: 117-127.

[4] White, B.S. & Fornberg, B. (1998) On the chance of freak waves at sea. J. Fluid Mech. 355 : 113-138.

[5] Pelinovsky, E. & Kharif, C. (2000) Simplified model of the freak wave formation from the random wave field. Proc. of the 15th International Workshop on Water Waves and Floating Bodies.

[6] Dysthe, K.B. & Trulsen, K. (1999) Note on breather type solutions of the NLS as models for freak-waves. Physica Scripta T82, 48-52.

[7] Onorato, M., Osborne, A.R. & Serio, M. (2002). Extreme wave events in directional, random oceanic sea states. Phys. Fluids. 14, 25-28.

[8] Lawton, G. (2001) New Scientist magazine, vol 170 issue 2297.

[9] ESA (European Space Agency) (2004) Ship-sinking monster waves revealed by ESA satellites.

[10] Dickison, D. (1995) Outside magazine, March.

[11] Vigor, J. (2000) "Planning for an unplanned inversion" in Good Old Boat Magazine: Vol. 3, N. 6, November/December.

[12] Smith, R. (1976) Giant waves. Fluid. Mech., vol. 77, part 3, pp. 417-431

[13] Kjeldsen, P. (2000) "A sudden disaster - in Extreme Waves". Proceedings of Rogue Waves (Brest 2000).

[14] Mallory J.K. (1975) "Abnormal waves off the South African coast - a danger to shipping." The Naval Architect, pp. 82-85.

[15] Anderson Chase G. http://www.bell.mma.edu/ achase/ NS-221-Big-Wave.html

[16] CNN (2005) http://www.cnn.com April the 18th.

[17] Dysthe, K.B. (1979) Note on a modification to the nonlinear Schrödinger equation for application to deep water waves. Proc. R. Soc. Lond. A 369, 105-114.

[18] Zakharov, V.E. (1968) Stability of periodic waves of finite amplitude on the surface of a deep fluid. J. Appl. Mech. Tech. Phys., 9, 190-194.

[19] Stiassnie, M. (1984) Note on the modified nonlinear Schrödinger equation for deep water wave. Wave Motion (6), 431-433.

[20] Trulsen, K. (2003) Real time deterministic ocean wave forecasting using weakly nonlinear wave evolution theory. In Proceedings of Computational Mechanics (MekIT'03), pp. 371-390. Tapir.

[21] Trulsen, K. & Dysthe, K. B. (1996) A modified nonlinear Schrödinger equation for broader bandwidth gravity waves on deep water. Wave Motion 24, 281-289.

[22] Trulsen, K., Kliakhandler, I., Dysthe, K. B & Velarde, M. G. (2000) On weakly nonlinear modulation of waves on deep water. Phys. Fluids 12, 2432-2437.

[23] Trulsen, K. & Dysthe, K. B. (1997) Frequency downshift in three-dimensional wave trains in a deep basin. J. Fluid Mech. 352, 359-373.

[24] Lo, E. & Mei, C. C. (1985). A numerical study of water-wave modulation based on a higher-order nonlinear Schrödinger equation. J. Fluid Mech. 150, 395-416.

[25] Tappert, F. (1974). Numerical Solutions of the Korteweg-de Vries Equation and its generalizations by the split-step Fourier method. Lectures Appl. Maths 15, 215-216.

[26] Fornberg, B. & Whitham, G.B. (1978). A numerical and theoritical study of certain nonlinear wave phenomena. Phil. Trans. R. Soc. Lond. A 289, 373-404.

[27] Trulsen, K. & Stansberg, C.T. (2001). Spatial evolution of water surface waves : Numerical simulation and experiment of bichromatic waves. In Proc. ISOPE 2001. 3, 71-77.

[28] Hasselman, K., Barnett, T.P., Bouws, E., Carlson, H., Cartwright, D.E., Euke, K., Ewing, J.A., Gienapp, H., Hasselman, D.E., Kruseman, P., Meerbrug, A., Müller, P., Olbers, D.J., Richter, K., Sell, W., & Walden, H. (1973). Measurements of wind-wave growth and swell decay during the Joint North Sea Wave Project (JONSWAP). Deutsches Hydr. Zeit., A 12, 1–95.

[29] Pierson, W.J., & Moskowitz, L. (1964) A proposed spectral form for fully developed wind seas based on the similarity theory of S.A. Kitaigorodskii. Jour. Geoph. Res., 69, 5181–5190.

[30] Haver, S., Eik, K.J, & Meling, T.S. (2002) On the prediction of wave crest height extremes.

[31] Torsethaugen, K. & Haver, S. (2004) Simplified double peak spectral model for ocean waves. Paper No. 2004-JSC-193

[32] Gunson, J. & Magnusson, A-K. (2002) Investigating conditions for rogue wave events from special wave observations and models. MAXWAVE project.

[33] Alber, I.E. (1978) The effects of randomness on the stability of two-dimensional surface wavetrains. Proc. R. Soc. Lond. A 363, 525-546.

[34] Alber, I.E. & Saffman, P.G. (1978) Stability of random nonlinear deep water waves with finite bandwith spectrum. TWR Defense and Spacesystems Group Rep. 32326-6035-RU-00

[35] Benjamin, T.B. & Feir, J.E. (1967) The desintegration of wave trains on deep water. Part 1. Theory. J. Fluid Mech. 27, 417-430.

[36] Crawford, D.R., Saffman, P.G. & Yuen H.C. (1980) Evolution of a random inhomogeneous field of nonlinear deep-water gravity waves. Wave Motion 2, 1-16.

[37] Hasselman, K. (1962) On the nonlinear energy transfer in a gravity wave-spectrum. Part 1. General theory. J. Fluid. Mech. 12, 481-500.

[38] Onorato, M., Osborne, A.R., Serio, M. & Damiani, T. (2000) Occurence of freak waves from envelope equations in random ocean wave simulations. Proceedings of the workshop Rogue Waves 2000 IFREMER. 181-191.

[39] Mori, N. & Yasuda, T. (2000) Effects of high-order nonlinear wave interactions on gravity waves. Proceedings of the workshop Rogue waves 2000 IFREMER. 229-244.

[40] Janssen, P.A.E.M. (2003) Nonlinear four wave interaction and freak waves. J. Phys. Oceanogr. 33, 863-884.

[41] Skourup, J., Andreasen, K.K. & Hansen, N.E.O. (1996) Non-Gaussian extreme waves in the central North Sea. OMAE, Vol I, part A, Offshore Technology. ASME 1996.

[42] Onorato, M., Osborne, A.R., Serio, M., Cavaleri, L., Brandini, C., & Stansberg, C.T. (2004) Extreme waves and modulational instability : wave flume experiments on irregular waves. Submitted to J. Fluid Mech.

[43] James Hu, S.-L. (2002) Nonlinearity and spectral width effects on ocean wave distribution. 15th ASCE Engineering Mechanics Conference.

[44] Longuet-Higgins, M.S. (1952) On the statistical distribution of the Heights of Sea Waves. Journal of Marine Research, Vol. XI, No.3, pp. 245-266.

[45] Tayfun, M.A (1980) Narrow-band nonlinear sea waves. Journal of Geophysical Research 85, 1548-1552.

[46] Cartwright, D.E. & Longuet-Higgins, M.S. (1956) The statistical distribution of the maxima of a random function. Prov. R. Soc. Lond. A. 237, 212-232.

[47] Forristall, G.Z. (1978) On the statistical distribution of wave heights in a storm. Journal of Geophysical Research 83(C5), 2353-2358.

[48] Longuet-Higgins, M.S. (1980) On the distribution of the heights of sea waves : Some effects on nonlinearity and finite bandwith. Journal of Geophysical Research 85(C3), 1519-1523.

[49] Naess, A. (1985) On the distribution of crest to trough wave heights. Ocean Engineering 12(3), 221-234.

[50] Mori, N., & Yasuda, Y. (2002) A weakly non-gaussian model of wave height distribution for random wave train. Ocean Engineering 29. 1219-1231

[51] Prevosto, M. & Forristall, G.Z. (2002) Statistics of wave crests from models vs. measurements. In Proc. of OMAE'O2, 21th Int. Conf. on Offshore Mechanics Artic Engineering, Oslo, Norway. OMAE2002-28443.

[52] Vinje, T. (1989) The statistical distribution of wave heights in a random seaway. Applied Ocean Research 11(3), 143-152.

[53] Tung, C.C., & Huang, N.E (1985) Peak and trough distributions of nonlinear waves. Ocean Engng, Vol 12, No. 3, 201-209.

[54] Tucker, M.J. (1991) Waves in Ocean Engineering; mesuarement, analysis, interpretation. Ellis Horwood Series in Marine Science.

[55] Warren, S.J., Bole, J.B. & Driver, D.B. (1998) Measured wave crest distributions in central and southern North Sea storms. Proceedings of Isope Conf. 1998. p. 96-102.

[56] Krunic, D. & Winterstein, S.R. (2000) Probabilistic Modelling of Extreme Wave Crests : A noisy Weibull Model. 8th ASCE Speciality Conference on Probabilistic Mechanics and Structural Reliability. PCM2000-342.

[57] Kriebel, D.L. & Dawson, T.H. (1991) Nonlinear effects on wave groups in random seas. Proc. 2nd Int. Symp. Ocean Wave Measurement and Analysis. 61-75.

[58] Leder, N., Smircic, A. & Vilibic, I. (1998) Extreme values of surface wave heights in the Northern Adriatic. Geofizika Vol. 15. UDC 551.46.06.

[59] Gumbel, E.J. (1958) Statistics of Extremes. Colombia University Press, New York.

[60] Fisher, R.A. & Tippett, L.H.C. (1928) Limiting forms of the frequency distribution of the largest or smallest member of a sample. Proc. Cambridge Philosophical Society, Vol 14, 180-190.

[61] Rice, S.O. (1944) Mathematical Analysis of random noise. Bell Syst. Techn. J. 23-24, 283-332 and 46-156.

[62] Piterbarg, V.I. (1996) Asymptotic Methods in the Theory of Gaussian Processes and Fields. AMS Transl. of Math. Monographs 148, Providence R.I.